EFFECTS OF CONVECTION ON SOUND RADIATION

By

Peter Leo Schmidt

Dissertation

Submitted to the Faculty of the

Graduate School of Vanderbilt University

in partial fulfillment of the requirements

for the degree of

DOCTOR OF PHILOSOPHY

in

Mechanical Engineering

August, 2006

Nashville, Tennessee

Approved:

Professor Kenneth D. Frampton

Professor Prodyot K. Basu

Professor Nilanjan Sarkar

Professor Alvin M. Strauss

Professor Mark A. Stremler

To my wife, Lisa Ann,

without whose love and support this would not have been possible

ACKNOWLEDGEMENTS

TABLE OF CONTENTS

LIST OF TABLES

LIST OF FIGURES

CHAPTER I

INTRODUCTION

Motivation

Radiation of sound into quiescent fluids from geometrically simple structures is well understood[1]. However, little has been done to investigate this behavior in convected fluids. Of the works that do consider this phenomenon, only a small number consider coupling between modes of the structure via the fluid medium being investigated.

It has been shown that fluid convection, coupled with structural motion, changes the way energy is radiated from, and absorbed by a structure[2,3,4,5].

The basic differential equation that governs the motion of any simple structure defines the relationship between lateral vibration of the structure and the lateral loading on that structure. Changing the loading on a structure changes the form of that equation. When a structure is under some type of stress resulting from external loading, it is prudent to assume that the dynamic behavior of that structure will change.

There are many different types of structure where the amount of energy emitted into the surrounding environment is of concern. Whether it is the noise transmitted into the cabin of an aircraft in flight or noise emitted by a submarine into the sea as a result of the action of the fluid flowing over the hull, the problem is governed by the same basic equations. The large difference in the physical parameters that describe these particular systems result in a need to quantify convection effects over a large range of fluid and structural parameter values in order to make judgments on when the effects of convection

should be included, but also when convection effects should be coupled to the structure to make accurate predictions of overall system performance.

Previous Work

Initial investigations into the effects of convection on radiation from structures have been done by Abrahams[2], Atalla and Nicolas[3], Graham[4] and Frampton[5]. Abrahams solves the convected wave equation using asymptotic techniques. His solution showed good agreement (within 2% for a large number of modes) with work done in the aeroelastic stability analysis community using Galerkin's Method[6]. Atalla and Nicolas expanded on earlier work by Berry[7] and used it to evaluate the radiation impedance for a rectangular piston in the presence of mean flow. Berry, Atalla and Nicolas used a Rayleigh-Ritz approach to describe the kinetic and potential energy of the structure. Atalla and Nicolas noted an increase in radiation efficiency as flow speed increased for both rectangular pistons and a plate vibrating in the (1, 1) and (2, 2) modes. Graham showed that the frequency at which any given mode becomes an efficient radiator decreases as flow velocity increases.

Frampton, expanding on work done by Currey and Cunefare[8] and by Wallace[9], chose to cast the problem in state variable form, with the structural dynamics discretized using Galerkin's Method and the aerodynamic model discretized using the methods developed by Dowell[10] for use in aeroelastic stability analysis. He showed that the radiation efficiency can be expressed as a transfer function in the frequency domain of the aerodynamic model, and that increases in flow speed increase the radiation efficiency

of any given structural mode. Frampton's findings are in agreement with the earlier work cited.

There are fewer references available that study the effects of flow induced intermodal coupling, including those of Sgard, Atalla and Nicolas[11], Wu and Maestrello[12] and Frampton[13]. Sgard, Atalla and Nicolas took the approach of discretizing the radiating structure with a FEM / BEM mixed approach. They showed that as flow speed increases, inter-modal coupling becomes a significant effect and must be considered when modeling the power radiated from a structure. They attribute the increase in radiated power as flow velocity increases to this effect. Wu and Maestrello also argue that flow induced coupling is an important part of the modeling of radiated acoustic power from structures into a convected fluid. Since their work was concerned with stability analysis, their discussion of radiated power was limited to the importance of it's inclusion in stability calculations, not it's behavior *per se*.

Frampton extended his earlier work with radiation efficiency to include the calculation of the kinetic energy of radiating structures and the associated radiated sound power when coupled with a convected fluid model. Earlier work by Fahy[14] was expanded to show that the kinetic energy and radiated power of the coupled system could be represented by transfer functions in the frequency domain. This work also concluded that coupling is important and that the power radiated by a structure into a convected fluid increased as flow velocity increased. Frampton included the important result that the coupling mechanism was the path to allow energy to be shared between modes of vibration in the structure, and that this mechanism accounted for the increased radiated

3

sound power as subsonic convection velocity increased. Frampton also noted that the kinetic energy of the structure remained nearly constant with varying flow velocities.

Purpose

The purpose of this work is to expand the work done by Frampton in three areas. First, the work with coupled structural and aerodynamic subsystems will be expanded to the supersonic flow region to quantify the effects on structural response and on radiated sound power behavior. Next, the method will be expanded by adding in-plane stresses to the structural system model, and exploring the effect that imposed stress has on the behavior of the structural response and radiated sound power for both subsonic and supersonic flow. These effects will be studied with the same physical parameter set used in the preceding work so that the effects observed may be compared and contrasted. Finally, the aerodynamic and structural subsystem models will be put in non-dimensional form such that a wide range of physical structural and fluid parameters may be studied. In this way, engineering rules of thumb can be derived for when the effects of convection and coupling must be considered for any specific case of fluid structure interaction likely to be encountered by structures operating in typical engineering applications.

CHAPTER II

THEORY

System Conceptual Model

The development begins by considering a finite, elastic, rectangular plate in an infinite baffle as depicted in Figure 2-1. On one side of the plate is a semi-infinite fluid, flowing parallel to the plane of the plate in the positive x-axis direction. The other side of the plate is exposed to a vacuum. As the plate vibrates a pressure disturbance is created in the convected fluid.

A mathematical model of this system begins with a modal description of the plate motion and the relationship of this motion to the dynamic behavior of the fluid. Next, the dynamics of the convected fluid are described by the convected wave equation. Given these coupled dynamic equations, a method for solving them is presented as is a method for computing the radiated sound power.
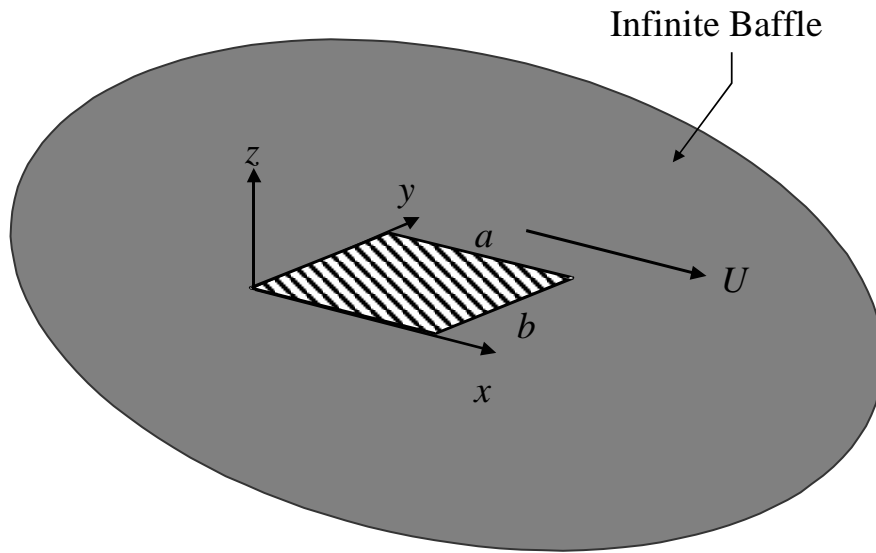
Figure 2-1.   Schematic of a plate in an infinite baffle

<div align="center">Structural Model</div>

Plate dynamics

The plate is modeled by employing Galerkin's technique to discretize the linear equations of motion[6]. The partial differential equation of motion for a thin, uniform plate is[15]:

$$0 = D\nabla^4 w(x, y,t) + \rho_s h_s \frac{\partial^2 w(x,t)}{\partial t^2} + p(x, y,t) + p_d(x, y,t), \qquad (2\text{-}1)$$

where *w(x,y,t), D, ρ* and *h* are the panel displacement, stiffness, density and thickness, respectively.   The plate is forced by the fluid and disturbance pressures, *p(x,y,t)* and *p_d(x,y,t)* respectively.

A separable solution is assumed using the *in vacuuo* panel eigenfunctions and generalized coordinates of the form:

$$w(x, y, t) = \sum_{n=1}^{N} \psi_n(x, y) q_n(t) \tag{2-2}$$

where, $\psi_n(x, y)$ is the mode shape and $q_n(t)$ is the generalized coordinate. The velocity of the plate can also be represented using the panel eigenfunctions and generalized coordinates as

$$\dot{w}(x, y, t) = \sum_{n=1}^{N} \psi_n(x, y) \dot{q}_n(t). \tag{2-3}$$

The approach presented here can accommodate any plate boundary condition. However, results will be presented for a simply supported plate, which has been shown to have the following mode shapes[15]:

$$\psi_n(x, y) = \sin\left(\frac{j\pi}{a} x\right) \sin\left(\frac{k\pi}{b} y\right), \tag{2-4}$$

where the nth plate mode has (x,y) directional indices (j,k).

Substituting Equation (2-2) and (2-4) into Equation (2-1) and multiplying by an arbitrary expansion function, $\psi_m(x, y)$, yields the homogeneous form:

$$D \sum_{n=1}^{N} \nabla^4 \psi_n \psi_m q_n + \rho \sum_{n=1}^{N} \psi_n \psi_m \ddot{q}_n = 0. \tag{2-5}$$

Equation (2-5) can be written in integral form for a single mode. The individual homogeneous equations are of the form:

$$D q_n \int_S \left(\nabla^4 \psi_n\right) \psi_m dS + \rho \ddot{q}_n \int_S \psi_n \psi_m dS = 0. \tag{2-6}$$

Equation (2-6) can be rewritten in the familiar form:

$$M_n \ddot{q}_n + K_n q_n = 0, \tag{2-7}$$

where

$$M_n = \rho \int_S \psi_n \psi_m dS \qquad (2\text{-}8)$$

and

$$K_n = D \int_S \left(\nabla^4 \psi_n \right) \psi_m dS . \qquad (2\text{-}9)$$

Substituting Equation (2-4) into (2-8) and (2-9) results in:

$$M_n = \rho \int_0^a \int_0^b \sin\left(\frac{m\pi x}{a}\right) \sin\left(\frac{n\pi y}{b}\right) \sin\left(\frac{j\pi x}{a}\right) \sin\left(\frac{k\pi y}{b}\right) dxdy \qquad (2\text{-}10)$$

and

$$K_n = D\pi^4 \left(\frac{m^2}{a} + \frac{n^2}{b}\right) \times$$
$$\int_0^a \int_0^b \sin\left(\frac{m\pi x}{a}\right) \sin\left(\frac{n\pi y}{b}\right) \sin\left(\frac{j\pi x}{a}\right) \sin\left(\frac{k\pi y}{b}\right) dxdy . \qquad (2\text{-}11)$$

Integrating over the domain using the stated boundary conditions yields

$$M_n = \frac{ab\rho}{4} \qquad (2\text{-}12)$$

and

$$K_n = \frac{D\pi^4 ab}{4} \left(\frac{m^2}{a} + \frac{n^2}{b}\right) \qquad (2\text{-}13)$$

for the diagonal terms , i.e., $m = n$. Equations (2-12) and (2-13) are identically equal to zero for $m \neq n$ due to the orthogonality of the mode shape functions. M_n is referred to as the modal mass term, and K_n is referred to as the modal stiffness term.

With these relationships in hand, a set of ordinary differential equations of the form:

$$0 = M_n [\ddot{q}_n(t) + 2\xi\omega_n \dot{q}_n(t) + \omega_n^2 q_n(t)] + Q_n(t) + Q_n^d(t) \qquad (2\text{-}14)$$

can be written. A damping term has been added to the non-homogeneous equation to account for energy dissipation in the structure.

In order to proceed with analysis of the structural system, parameters that characterize the structure must be selected. For this analysis, plate geometry is chosen that is representative of a physical system that may be exposed to the flow speeds and fluid properties that will be investigated. The dimensions of the plate will be assumed to be 1 meter in the direction of flow (x direction) and 0.83 meters in the direction perpendicular to the flow (y direction). For the non-dimensional portion of the study, physical dimensions are removed from the structural model, but the aspect ratio of the plate, defined as

$$\eta = \frac{a}{b},$$
(2-15)

is retained from the dimensions assumed.

Fixing the aspect ratio of the plate fixes the modal indices of the plate resonances[15]. This is true for all variations of the structural model considered here. While the resonance frequencies will change based on changes to the structural model, the uncoupled mode shapes will remain the same. For this analysis, a model that includes the first 20 mode shapes of the structure will be used. Figures 2-2, 2-3 and 2-4 provide visualizations for selected mode shapes.

Table 2-1.   Modal Indices of the Structural Model

Mode Number	Indices(j,k)	Mode Number	Indices(j,k)
1	(1,1)	11	(3,3)
2	(2,1)	12	(1,4)
3	(1,2)	13	(5,1)
4	(2,2)	14	(2,4)
5	(3,1)	15	(4,3)
6	(1,3)	16	(5,2)
7	(3,2)	17	(3,4)
8	(2,3)	18	(1,5)
9	(4,1)	19	(6,1)
10	(4,2)	20	(5,3)
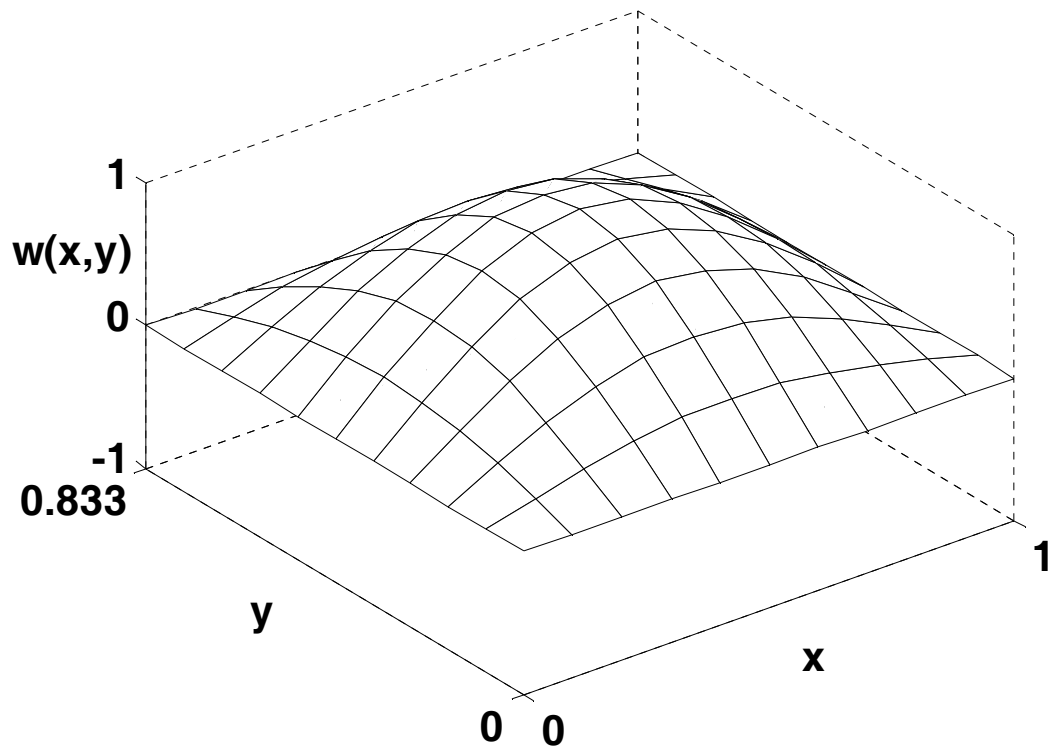
Figure 2-2.   Visualization of the (1, 1) mode
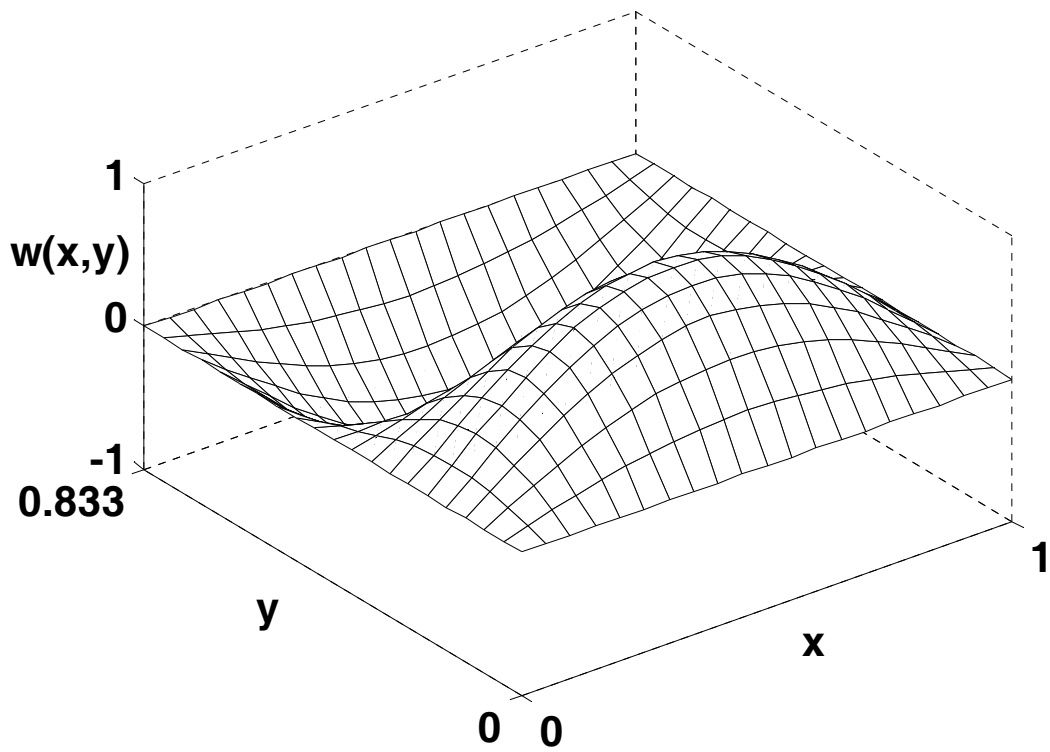
Figure 2-3.   Visualization of the (1, 2) mode
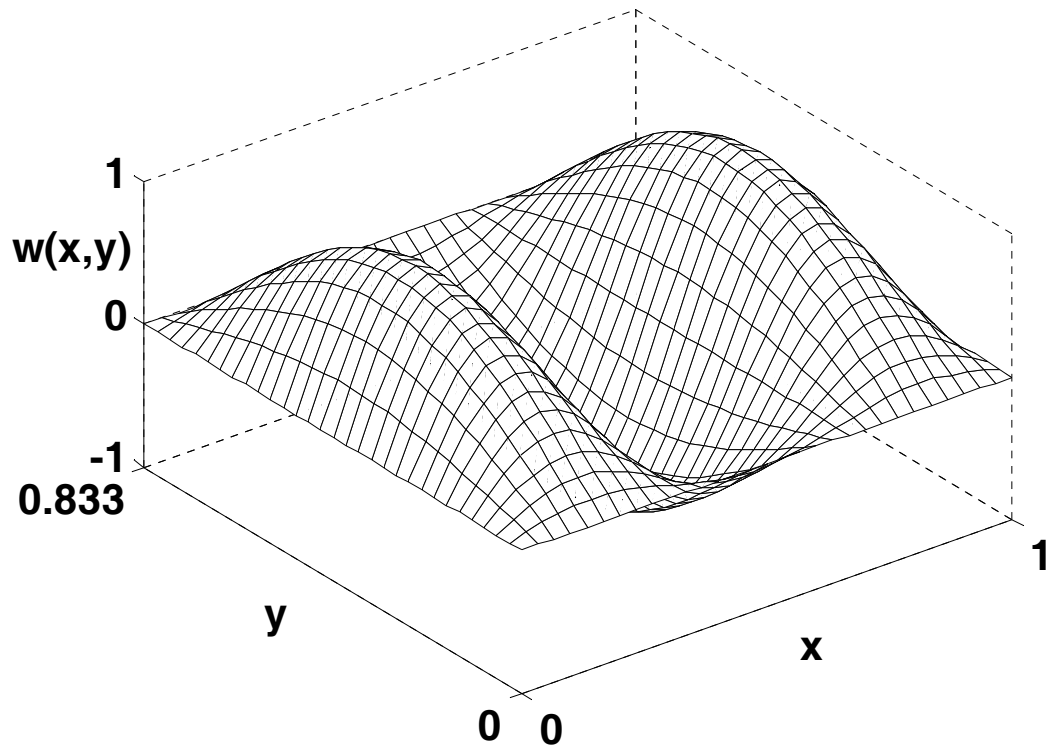
Figure 2-4.   Visualization of the (3, 1) mode

Structural Dynamics with In-plane Stresses

The partial differential equation of motion for a thin, uniform plate subjected to in-plane forces is[15]:

$$
\begin{aligned}
D\nabla^4 w(x,y,t) + \rho_s h_s \frac{\partial^2 w(x,y,t)}{\partial t^2} + p(x,y,t) + p_d(x,y,t) = \\
N_x \frac{\partial^2 w(x,y,t)}{\partial x^2} + 2N_{xy}\frac{\partial^2 w(x,y,t)}{\partial x\,\partial y} + N_y \frac{\partial^2 w(x,y,t)}{\partial y^2},
\end{aligned}
\tag{2-16}
$$

where *w(x,y,t), D, ρ* and *h* are the panel displacement, stiffness, density and thickness respectively. N_x and N_y are the normal stresses in the indicated directions and N_{xy} is the shear stress on the plate. The plate is forced by the fluid and disturbance pressures,

12

$p(x,y,t)$ and $p_d(x,y,t)$ respectively. For this work, it will be assumed that there is no shear stress acting on the plate ($N_{xy} = 0$).

This equation can be reduced to the form of Equation (2-14) in a similar fashion as shown in the previous section. However, for the case of in-plane stress, it should be noted that the terms denoting the resonant frequencies in Equation (2-14) are no longer functions strictly of the mass and stiffness of the basic structural system, but involve N_x and N_y, such that:

$$\omega_n = \sqrt{\frac{D\pi^4}{\rho_s}\left(\frac{m_j^2}{a^2} + \frac{n_k^2}{b^2}\right) + \frac{N_x m_j^2 \pi^2}{\rho_s a^2} + \frac{N_y n_k^2 \pi^2}{\rho_s b^2}} = \sqrt{\frac{K_n^s}{M_n^s}}. \quad (2\text{-}17)$$

Non-dimensional Structural Model

Equation (2-14) can also be placed in non-dimensional form by utilizing the following relationships:

$$\mu = \frac{\rho_\infty a}{\rho_s h} \quad (2\text{-}18)$$

$$\lambda = \frac{U_\infty^2 \rho_\infty a^3}{D} \quad (2\text{-}19)$$

$$s = t\left(\frac{U_\infty}{a}\right) \quad (2\text{-}20)$$

$$r_n(s) = \frac{q_n(t)}{h} \quad (2\text{-}21)$$

and

$$\hat{Q}_n(s) = \frac{Q_n(t)}{U_\infty^2 \rho_\infty bh} \quad (2\text{-}22)$$

13

where ρ_∞ is the density of the fluid, μ is the mass ratio, U_∞ is the convection velocity, λ is the non-dimensional dynamic pressure, s is dimensionless time, r is dimensionless plate generalized displacement and $\hat{Q}_n(s)$ is dimensionless plate generalized force. Utilizing these relationships, we can recast Equation (2-14) as:

$$\ddot{r}(s) + \pi^4 \frac{\mu}{\lambda}\left(j^2 + \eta^2 k^2\right)^2 r(s) + 4\mu\left(\hat{Q}_n(s) + \hat{Q}_n^d(s)\right) = 0. \quad (2\text{-}23)$$

State Space Form of the Structural Model

Equations (2-14) and (2-23) actually represent N simultaneous ordinary differential equations where N is the number of structural modes used in the solution. In order to facilitate integration of Equation (2-14) with the fluid dynamics, it is cast in state variable form such that[16]

$$\begin{aligned}
\dot{\mathbf{x}}_\mathbf{s} &= \mathbf{A}_\mathbf{s}\mathbf{x}_\mathbf{s} + \mathbf{B}_\mathbf{s}\mathbf{u}_\mathbf{s} \\
\mathbf{y}_\mathbf{s} &= \mathbf{C}_\mathbf{s}\mathbf{x}_\mathbf{s}
\end{aligned} \quad (2\text{-}24)$$

The $\mathbf{A_s}$ and $\mathbf{B_s}$ matrices are populated with the coefficients of Equation (2-14) while the state, input and output vectors $\mathbf{x_s}$, $\mathbf{u_s}$ and $\mathbf{y_s}$ are defined as

$$\mathbf{x}_\mathbf{s} = \left\{ q_1(t) \cdots q_N(t) \; \dot{q}_1(t) \cdots \dot{q}_N(t) \right\}^T, \quad (2\text{-}25)$$

$$\mathbf{u}_\mathbf{s} = \left\{ Q_1(t) \cdots Q_N(t) \; Q_1^d(t) \cdots Q_N^d(t) \right\}^T \quad (2\text{-}26)$$

and

$$\mathbf{y}_\mathbf{s} = \mathbf{x}_\mathbf{s} = \left\{ q_1(t) \cdots q_N(t) \; \dot{q}_1(t) \cdots \dot{q}_N(t) \right\}^T. \quad (2\text{-}27)$$

Similarly, for the non-dimensional model, these relationships are:

$$\mathbf{x}_\mathbf{s} = \left\{ r_1(s) \cdots r_N(s) \; \dot{r}_1(s) \cdots \dot{r}_N(s) \right\}^T, \quad (2\text{-}28)$$

$$\mathbf{u_s} = \{ \hat{Q}_1 \cdots \hat{Q}_N(s) \; \hat{Q}_1^d(s) \cdots \hat{Q}_N^d(s) \}^T \tag{2-29}$$

and

$$\mathbf{y_s} = \mathbf{x_s} = \{ r_1(s) \cdots r_N(s) \; \dot{r}_1(s) \cdots \dot{r}_N(s) \}^T . \tag{2-30}$$

The disturbance generalized forces in all cases are given by

$$Q_n^d(t) = \int_0^b \int_0^a p_d(x, y, z = 0, t) \psi_n(x, y) \, dx \, dy , \tag{2-31}$$

and the fluid generalized forces are defined by

$$Q_n(t) = \int_0^b \int_0^a p(x, y, z = 0, t) \psi_n(x, y) \, dx \, dy , \tag{2-32}$$

where $p_a(x,y,z=0,t)$ is the fluid pressure acting on the plate due to plate motion and $Q_n(t)$ is the resulting generalized force. This generalized force is due entirely to the fluid response created by plate motion and is therefore the mechanism through which modal coupling is created. Developing an expression for this generalized force is the next step toward studying the effects of flow on sound radiation.

Aerodynamic Model

Fluid Dynamics

Other investigators have used two differing approaches to find the acoustic pressure that acts on the surface of a vibrating plate. One approach is the Helmholtz-Kirchoff integral, typically solved using numerical methods[3,9,11]. The alternate method involves spatial Fourier transform techniques that require approximated inverse transforms derived using asymptotic techniques[2,4]. The approach detailed here is based on the Fourier transform method.

15

The generalized forces due to aerodynamic pressure in Equation (2-14) are obtained by solving the partial differential equation that describes the velocity potential in an inviscid, irrotational fluid flow in the x direction, as shown in Figure 2-1. This relationship is also known as the convected wave equation.

$$\nabla^2 \Phi - \frac{1}{c^2}\frac{\partial^2 \Phi}{\partial t^2} + 2U\frac{\partial^2 \Phi}{\partial t\,\partial x} + U^2\frac{\partial^2 \Phi}{\partial x^2} = 0 \qquad (2\text{-}33)$$

Equation (2-33) is subject to the boundary conditions for a plate embedded in an infinite baffle,

$$\left.\frac{\partial \Phi}{\partial z}\right|_{z=0} = \begin{array}{l} U\dfrac{\partial w}{\partial x} + \dfrac{\partial w}{\partial t} \quad \text{on the plate} \\ 0 \qquad\qquad\qquad \text{off the plate} \end{array}, \qquad (2\text{-}34)$$

as well as a finiteness condition as z approaches infinity. Here, Φ, c, and U are the velocity potential, speed of sound and flow velocity respectively.

The solution to these equations follows the one presented by Dowell[10], and summarized by Frampton[5]. The first step is to perform a double Fourier transform with respect to the x and y spatial dimensions and a Laplace transform with respect to time according to the following relationships:

$$\tilde{\Phi}(\alpha,\gamma,z,s) = \int_{-\infty}^{\infty}\int_{-\infty}^{\infty} e^{-(\alpha x + \gamma y)}\,\Phi(x,y,z,s)\,dx\,dy \qquad (2\text{-}35)$$

$$\Phi(x,y,z,s) = \int_{0}^{\infty} e^{-st}\phi(x,y,z,t)\,dt. \qquad (2\text{-}36)$$

If these relationships are applied to Equation (2-33), the following is obtained:

$$\frac{d^2\tilde{\Phi}}{dz^2} = \tilde{\Phi}\mu^2 \qquad (2\text{-}37)$$

where

16

$$\mu = \sqrt{\frac{s^2}{c^2} + \frac{2Msi\alpha}{c} - \alpha^2(M^2 - 1) + \gamma^2},\qquad (2\text{-}38)$$

and where s is the Laplace transform variable, $M = \dfrac{U}{c}$ is the Mach number, $i = \sqrt{-1}$,

and α and γ are the Fourier transform variables in x and y. The triple transform of the

boundary conditions is obtained in a similar way, resulting in:

$$\frac{d^2\tilde{\Phi}}{dz^2} = \tilde{F}.\qquad (2\text{-}39)$$

This transformed version of the convected wave equation (Equation 2-33), when

solved with the transformed boundary condition of Equation (2-39), yields the

transformed velocity potential on the plate surface, which is given by

$$\tilde{\Phi}\Big|_{z=0} = \frac{-\tilde{F}}{\mu}.\qquad (2\text{-}40)$$

If an inverse Laplace transform is taken of Equation (2-40), then the result is the velocity

potential in the time domain on the surface of the plate,

$$\tilde{\phi}(x, y, z = 0, t) = -c\int_0^t \tilde{f}(\alpha, \gamma, \tau) e^{-iMc\alpha(t-\tau)} \times$$
$$J_0\left[\left(\alpha^2 + \gamma^2\right)^{\frac{1}{2}} c(t - \tau)\right] d\tau.\qquad (2\text{-}41)$$

where $J_k[\bullet]$ is a Bessel function of the first kind and of order k and τ is a variable of

integration.

In order to calculate aerodynamic forces on the plate, the pressure on the surface

of the plate is needed. The velocity potential is related to the acoustic pressure through

Bernoulli's equation,

$$p = -\rho\frac{\partial\Phi}{\partial t} + U\frac{\partial\Phi}{\partial x}.\qquad (2\text{-}42)$$

where ρ is the density of the fluid. If Equations (2-41) and (2-42) are combined, the result is:

$$\tilde{p}(\alpha, \gamma, z = 0, t) = \rho c \tilde{f}(t) - \rho c^2 \sqrt{(\alpha^2 + \gamma^2)} \times$$

$$\int_0^t \tilde{f}(t) e^{-iMc\alpha(t-\tau)} J_1 \left[c(\alpha^2 + \gamma^2)^{\frac{1}{2}}(t-\tau) \right] d\tau \qquad (2\text{-}43)$$

An inverse Fourier transform of Equation (2-43) can now be performed. A logarithmic singularity exists for subsonic flows at the leading edge of the plate. This presents problems if it is necessary to determine pressures at this specific location. For this work, there is only a need to calculate the generalized force due to the aerodynamic pressure over the entire surface of the plate.

The next step is to substitute Equation (2-43) into Equation (2-42). Integration with respect to the x and y coordinates is performed next, followed by an inverse Fourier integration with respect to α and γ. By performing the integrations in this order, the singularity at the leading edge of the plate is avoided. This series of operations results in an expression for the generalized forces on the plate such that

$$Q_n = \sum_{m=1}^{N} Q_{mn}(t), \qquad (2\text{-}44)$$

where $Q_{mn}(t)$ is the force on the nth panel mode due to the motion of the mth panel mode. The expression for $Q_{mn}(t)$ is given by:

$$Q_{mn}(t) = \sum_{m=1}^{N} \left[q_m(t) S_{mn} + \dot{q}_m(t) D_{mn} \right]$$

$$+ \sum_{m=1}^{N} \left[\int_0^t q_m(\tau) H_{mn}(t - \tau) d\tau \right] \qquad (2\text{-}45)$$

$$+ \sum_{m=1}^{N} \left[\int_0^t \dot{q}_m(\tau) I_{mn}(t - \tau) d\tau \right],$$

18

with

$$S_{mn} = \frac{1}{M} \int_0^a \int_0^b \frac{\partial \psi_m}{\partial x} \psi_n \, dx \, dy, \tag{2-46}$$

$$D_{mn} = \frac{1}{MU} \int_0^a \int_0^b \psi_m \psi_n \, dx \, dy, \tag{2-47}$$

$$H_{mn} = \frac{U}{4\pi^2 M^2} \int_{-\infty}^{\infty} \int_{-\infty}^{\infty} G_{mn} i\alpha \sqrt{\alpha^2 + \gamma^2} e^{-i\alpha Ut} \times \\ J_1\left(ct\sqrt{\alpha^2 + \gamma^2}\right) d\alpha \, d\gamma, \tag{2-48}$$

$$I_{mn} = \frac{1}{4\pi^2 M^2} \int_{-\infty}^{\infty} \int_{-\infty}^{\infty} G_{mn} \sqrt{\alpha^2 + \gamma^2} e^{-i\alpha Ut} \times \\ J_1\left(ct\sqrt{\alpha^2 + \gamma^2}\right) d\alpha \, d\gamma, \tag{2-49}$$

$$G_{mn} = \int_0^a \int_0^b \psi_m e^{-i(\alpha x + \gamma y)} \, dx \, dy \times \int_0^a \int_0^b \psi_n e^{i(\alpha x + \gamma y)} \, dx \, dy. \tag{2-50}$$

S_{mn} and D_{mn} are referred to as aerodynamic influence coefficients. These terms relate instantaneous changes in structural generalized coordinates to instantaneous changes in the generalized forces due to aerodynamic pressure. The influence coefficients (Equations 2-46 and 2-47) can be obtained analytically for most plate eigenfunctions. The same is true of Equation (2-50)[5].

The aerodynamic influence functions, $H_{mn}(t)$ and $I_{mn}(t)$, are defined by integrals with no known closed form solution. Dowell[10] used numeric integration to find the influence functions, and then used numeric time stepping algorithms to simulate the system response. This approach worked well for Dowell's area of interest, stability analysis. This work depends on the ability to perform eigenvalue analysis, similar to that done by Currey and Cunefare[8]. This necessitates the use of singular value decomposition technique, which results in a state variable representation of the fluid dynamic model.

This approach allows one to represent the relationship between the motion of the structure and the generalized forces in transfer function form.

Approximation of the Aerodynamic Generalized Forces

In order to approximate the aerodynamic generalized forces, a singular value decomposition (SVD) technique originally developed as a system identification tool is applied[17]. This SVD method uses time domain impulse responses to obtain the system representation. Since the aerodynamic influence functions, $H_{mn}(t)$ and $I_{mn}(t)$, are essentially impulse responses of the aerodynamic model, the SVD method is easily applied to the problem at hand. This SVD method also has the advantage of producing a model in state variable form, which is the desired formulation here. This approach also allows the use of standard system analysis tools available based on linear systems theory.

Since a state space model of the aerodynamic subsystem is desired, Equation (2-45) must be rewritten in the proper form. Equation (2-45) is a mapping of the relationship between the motion of the structure and the aerodynamic forces. This relationship can be expressed in the following form:

$$\mathbf{x}((k+1)T) = \mathbf{A}\mathbf{x}(kT) + \mathbf{B}\mathbf{u}(kT),$$

$$\mathbf{y}((k+1)T) = \mathbf{C}\mathbf{x}(kT) + \mathbf{D}\mathbf{u}(kT),$$
(2-51)

where T is the discrete time increment and k is the time index. The state variable system ($\mathbf{A}$,$\mathbf{B}$,$\mathbf{C}$,$\mathbf{D}$) has n states in $\mathbf{x}$, p inputs in $\mathbf{u}$ and m outputs in $\mathbf{y}$. For the structure considered here with N modes included in the model expansion, the input ($\mathbf{u}$) and output ($\mathbf{y}$) vectors take the form

$$\mathbf{u} = \begin{bmatrix} q_1 & q_2 & \cdots & q_N & \dot{q}_1 & \dot{q}_2 & \cdots & \dot{q}_N \end{bmatrix}$$
(2-52)

and

$$\mathbf{y} = \begin{bmatrix} Q_1 & Q_2 & \cdots & Q_N \end{bmatrix}.$$ (2-53)

The first step in constructing that state variable model of the aerodynamic system is to build a block Hankel matrix of the system impulse responses. The basic form of this matrix is

$$\mathbf{H} = \begin{bmatrix} \mathbf{h}(T) & \mathbf{h}(2T) & \mathbf{h}(3T) & \cdots & \mathbf{h}((J+1)T) \\ \mathbf{h}(2T) & \mathbf{h}(3T) & \mathbf{h}(4T) & \cdots & 0 \\ \mathbf{h}(3T) & \mathbf{h}(4T) & \mathbf{h}(5T) & \cdots & 0 \\ \vdots & \vdots & \vdots & \ddots & \vdots \\ \mathbf{h}((J+1)T) & 0 & 0 & \cdots & 0 \end{bmatrix},$$ (2-54)

where the individual elements of the matrix are given by:

$$\mathbf{h}(kT) = \begin{bmatrix} S_{11} & S_{21} & \cdots & S_{N1} & D_{11} & D_{21} & \cdots & D_{N1} \\ S_{12} & S_{22} & \cdots & S_{N2} & D_{11} & D_{22} & \cdots & D_{N2} \\ \vdots & \vdots & \ddots & \vdots & \vdots & \vdots & \ddots & \vdots \\ S_{1N} & S_{2N} & \cdots & S_{NN} & D_{1N} & D_{2N} & \cdots & D_{NN} \end{bmatrix}$$

for $k = 0$

$$= \begin{bmatrix} H_{11}(kT) & \cdots & H_{N1}(kT) & I_{11}(kT) & \cdots & I_{N1}(kT) \\ H_{12}(kT) & \cdots & H_{N2}(kT) & I_{12}(kT) & \cdots & I_{N2}(kT) \\ \vdots & \ddots & \vdots & \vdots & \ddots & \vdots \\ H_{1N}(kT) & \cdots & H_{NN}(kT) & I_{1N}(kT) & \cdots & I_{NN}(kT) \end{bmatrix}$$ (2-55)

for $k = 1, 2, ..., J+1$

$$= \begin{bmatrix} 0 \end{bmatrix}$$

for $k > J+1$.

This results in a Hankel matrix $\mathbf{H}$ with dimensions $m(J+1)$ by $p(J+1)$.

The next step is to perform the SVD operation on the matrix $\mathbf{H}$. This operation yields

$$\mathbf{H} = U\Sigma V^T = \mathbf{U}\mathbf{V}^T,$$ (2-56)

where **U** is an orthogonal matrix containing the eigenvectors of $\mathbf{HH}^T$, of dimension $m(J+1)$ by $(J+1)$, **V** is an orthogonal matrix containing the eigenvectors of $\mathbf{H}^T\mathbf{H}$, of dimension $p(J+1)$ by $(J+1)$, and the singular value matrix is given by:

$$
\Sigma = \begin{bmatrix}
\sigma_1 & & & & & & & \\
& \sigma_2 & & & & & 0 & \\
& & \ddots & & & & & \\
& & & \sigma_r & & & & \\
& & & & \varepsilon_{r+1} & & & \\
& & & & & \varepsilon_{r+2} & & \\
& 0 & & & & & \ddots & \\
& & & & & & & \varepsilon_{J+1}
\end{bmatrix}
\tag{2-57}
$$

such that the singular values are arranged in descending order,

$$
\sigma_1 \geq \sigma_2 \geq \cdots \sigma_r \geq \varepsilon_{r+1} \geq \varepsilon_{r+2} \geq \cdots \varepsilon_{J+1},
\tag{2-58}
$$

with

$$
\mathbf{U} = U\Sigma^{\frac{1}{2}}, \text{ and } \mathbf{V} = \Sigma^{\frac{1}{2}}V^T.
\tag{2-59}
$$

If the matrix **H** has a rank of r, then the singular values $\varepsilon_{r+1}, \varepsilon_{r+2}, \cdots, \varepsilon_{J+1}$ are equal to zero. If these singular values are non-zero, but very small, **H** has a rank very near to r. In this case, the small singular values represent degrees of freedom with negligible contribution to the system response or slight computational noise in the system impulse response. This property of the system realization is used in selecting the order of the final model.

Reduced Order System Model

A reduced order system, $\left(\hat{\mathbf{A}}, \hat{\mathbf{B}}, \hat{\mathbf{C}}, \hat{\mathbf{D}}\right)$, which discards excess degrees of freedom is created. This new system model, of order r, can be obtained by partitioning the output of the SVD operation as

$$
\mathbf{H} = \begin{bmatrix} \mathbf{U}_{1,1} & \mathbf{U}_{1,2} \\ \mathbf{U}_{2,1} & \mathbf{U}_{2,2} \\ \vdots & \vdots \\ \mathbf{U}_{J,1} & \mathbf{U}_{J,2} \\ \mathbf{U}_{J+1,1} & \mathbf{U}_{J+1,2} \end{bmatrix} \begin{bmatrix} \mathbf{V}_{1,1}^{T} & \mathbf{V}_{2,1}^{T} & \cdots & \mathbf{V}_{J,1}^{T} & \mathbf{V}_{J+1,1}^{T} \\ \mathbf{V}_{1,2}^{T} & \mathbf{V}_{2,2}^{T} & \cdots & \mathbf{V}_{J,2}^{T} & \mathbf{V}_{J+1,2}^{T} \end{bmatrix},
\tag{2-60}
$$

where the block matrices $\mathbf{U}$ and $\mathbf{V}$ are sized as follows:

$$
\begin{aligned}
&\mathbf{U}_{i,1} \text{ are } m \text{ by } r \\
&\mathbf{U}_{i,2} \text{ are } m \text{ by } J + r - 1 \\
&\mathbf{V}_{i,1} \text{ are } p \text{ by } r \\
&\mathbf{V}_{i,2} \text{ are } p \text{ by } J + r - 1 \\
&i = 1 : J + 1.
\end{aligned}
\tag{2-61}
$$

Based on these relationships, the reduced order system model is defined as:

$$
\hat{\mathbf{A}} = \left(\begin{bmatrix} \mathbf{U}_{1,1} \\ \mathbf{U}_{2,1} \\ \vdots \\ \mathbf{U}_{J,1} \end{bmatrix}^{T} \begin{bmatrix} \mathbf{U}_{1,1} \\ \mathbf{U}_{2,1} \\ \vdots \\ \mathbf{U}_{J,1} \end{bmatrix} \right)^{-1} \begin{bmatrix} \mathbf{U}_{1,1} \\ \mathbf{U}_{2,1} \\ \vdots \\ \mathbf{U}_{J,1} \end{bmatrix}^{T} \begin{bmatrix} \mathbf{U}_{2,1} \\ \mathbf{U}_{3,1} \\ \vdots \\ \mathbf{U}_{J+1,1} \end{bmatrix},
\tag{2-62}
$$

$$
\hat{\mathbf{B}} = \mathbf{V}_{1,1}^{T},
\tag{2-63}
$$

$$
\hat{\mathbf{C}} = \mathbf{U}_{1,1},
\tag{2-64}
$$

and

$$
\hat{\mathbf{D}} = \mathbf{h}(0).
\tag{2-65}
$$

This reduced order aerodynamic model will receive inputs from the structural subsystem and provide output both to the structure and for use in analysis. It should be noted that the formulation of the reduced order model renders the states of the model as mathematical constructs with no simple physical meaning.

<u>Subsystem Coupling</u>

The Coupled Model

The plate and fluid systems in state variable form can be assembled into a coupled fluid/structure system as shown in Figure 2-5. Note that this fluid/structure coupling is created by the dependence of the fluid generalized forces on the plate motion. So, motion in the plate creates a response in the fluid, which in turn creates a force back on the plate. Furthermore, when cast in the form shown in Figure 2-5, the input/output relationships for the system can be easily manipulated and transfer functions between inputs and system variables can be obtained. This feature of state variable modeling is important to for the calculation of surface velocity, radiated sound power and radiation efficiency of the structure.

In order to quantify coupling, it is important to clarify the language used to describe the structural response. The term "*in vacuuo* mode" will be used to describe the plate eigenfunctions of Equation (2-4). (The *in vacuuo* modes could be more accurately called comparison functions[6] since, in the fully coupled system, they are really just mathematically convenient functions with which to solve the differential equation.) The

modes of the fully coupled system shown in Figure 2-5 will be referred to as *coupled modes*. These are the structural mode shapes that result from solving the eigenvalue problem of the coupled fluid/structure system. Each coupled mode includes degrees of freedom associated with the plate and with the fluid.
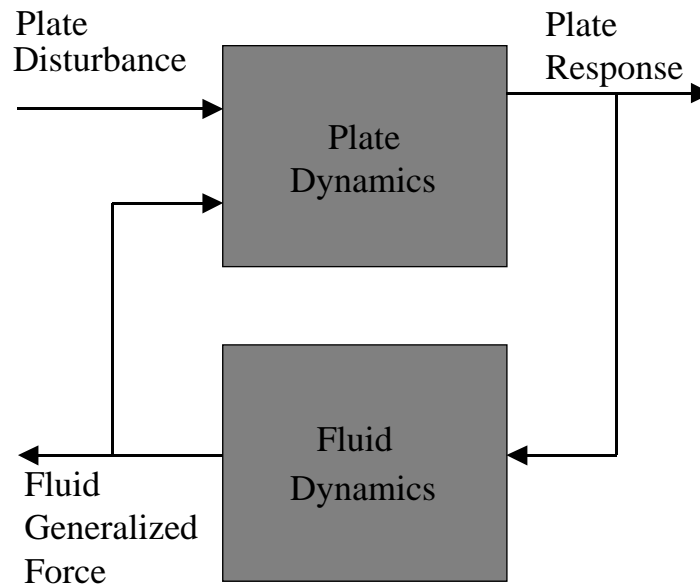
Figure 2-5.   Schematic of the coupled fluid / structure system

Structural Response Relationships

Kinetic Energy

In this work, the kinetic energy of the structure in the frequency domain will be an important quantity used in calculating acoustical behavior. The equation for kinetic energy is

$$T(\omega) = \frac{1}{2} m \dot{w}(\omega)^2 \tag{2-66}$$

where m is the mass of the plate. For a simply supported plate, with substitutions according to Galerkin's method, the modal mass term is given by Equation (2-12). Equation (2-12) is substituted into Equation (2-66) to yield

$$T(\omega) = \frac{ab\rho_s}{8} \dot{w}(\omega)^2 . \tag{2-67}$$

for each mode of vibration. Since our model is in state variable form, a transfer function relationship exists for the structural surface velocity. Frampton[5] showed that Equation (2-67) can be written as

$$T(\omega) = \frac{ab\rho_s}{4} \sum_{i=1}^{N} \left\| H_{d\dot{q}_i}(\omega) \right\|^2 I_{dd}(\omega), \tag{2-68}$$

where $H_{d\dot{q}_i}$ is the transfer function between an external system disturbance and the generalized plate velocity, and I_{dd} is the frequency content of the external disturbance. For this work, the disturbance will be white noise, such that $I_{dd} = 1$. This leads to

$$T(\omega) = \frac{ab\rho_s}{4} \sum_{i=1}^{N} \left\| H_{d\dot{q}_i}(\omega) \right\|^2 . \tag{2-69}$$

While this disturbance is not necessarily physically realistic, it does provide a worst case for analysis. It also provides information strictly about the frequency response of the structure, independent of external excitation.

Average Velocity

Another aspect of structural response of interest is the spatio-temporal average over the entire surface of the structure. This quantity can also be determined for a simply supported plate analytically. Frampton[5] showed that

$$\left\langle \left| \dot{q}_N \right|^2 \right\rangle = \frac{1}{8} \tilde{\dot{q}}_N^2 , \tag{2-70}$$

where $\tilde{\dot{q}}_N$ is the complex amplitude of the generalized velocity of the plate for a single mode of vibration.

Radiated Sound Power Relationships

The instantaneous sound power radiated from a plate vibrating in it's n^{th} mode can be expressed as

$$\Pi_n(t) = \int_S p_n(x, y, z = 0, t)\, \dot{w}_n(x, y, t)\, dS , \tag{2-71}$$

where $p_n(x, y, z = 0, t)$ is the pressure on the plate created by the nth mode of vibration and $\dot{w}_n(x, y, t)$ is the velocity of the plate due to the motion of the nth mode of vibration. Substituting Equation (2-3) for the velocity of the plate yields

$$\Pi_n(t) = \dot{q}_n(t)\int_S p_n(x, y, z = 0, t)\, \psi_n(x, y)\, dS. \tag{2-72}$$

The integral term in Equation (2-72) is equivalent to Equation (2-32), so

$$\Pi_n(t) = Q_n(t)\dot{q}_n(t). \tag{2-73}$$

Harmonic motion of the structure will be assumed. With this assumption, Equation (2-2) can be written as

$$w(x, y, t) = \psi_n(x, y) \tilde{q}_n e^{j\omega t}, n = 1, 2, \ldots, N \qquad (2\text{-}74)$$

where $\tilde{q}_n$ is the complex modal amplitude of the generalized displacement and ω is the driving frequency. Using this relationship, Equation (2-73) can be written as

$$\Pi_n(t) = \tilde{Q}_n \tilde{\dot{q}}_n e^{j\omega t}, \qquad (2\text{-}75)$$

where $\tilde{\dot{q}}_n$ is the complex modal velocity magnitude $(j\omega \tilde{q}_n)$, and $\tilde{Q}_n$ is the complex modal generalized force magnitude. The total instantaneous radiated power is then given by:

$$\Pi(t) = \sum_{n=1}^{N} \tilde{Q}_n \tilde{\dot{q}}_n e^{j\omega t}. \qquad (2\text{-}76)$$

The standard relationship[18] for time averaged acoustic power is given by

$$\langle \Pi \rangle = \frac{1}{T} \int_0^T \vec{F} \, \vec{v} \, dt, \qquad (2\text{-}77)$$

where T is the sampling period. In this case, Equation (2-77) can be written:

$$\langle \Pi \rangle = \frac{1}{T} \int_0^T \sum_{n=1}^{N} Q_n(t) \, \dot{q}_n(t) \, dt. \qquad (2\text{-}78)$$

Since harmonic motion is assumed, and realizing $T = \dfrac{2\pi}{\omega}$, Equation (2-78) becomes[18]:

$$\begin{aligned}
\langle \Pi \rangle &= \sum_{n=1}^{N} \frac{1}{T} \int_0^{\frac{2\pi}{\omega}} \Re\{\tilde{Q}_n e^{j\omega t}\} \Re\{\tilde{\dot{q}}_n e^{j\omega t}\} \, dt \\
&= \frac{1}{2} \sum_{n=1}^{N} \Re\{\tilde{Q}_n \tilde{\dot{q}}_n^*\}.
\end{aligned} \qquad (2\text{-}79)$$

Since a state variable model has been constructed, the transfer functions between an external disturbance and the nth generalized force input and between an external disturbance and the nth generalized velocity output are available. These transfer functions allow Equation (2-79) to be written as:

$$\langle \Pi \rangle = \frac{1}{2} \sum_{n=1}^{N} \Re \{ H_{dQ}(\omega) H_{d\dot{q}}^{*}(\omega) \} | I_{dd}(\omega) |^{2} \qquad (2\text{-}80)$$

where $H_{dQ}(\omega)$ is the transfer function between the external disturbance and the generalized force acting on the nth mode, $H_{d\dot{q}}^{*}(\omega)$ is the transfer function between the external disturbance and the generalized velocity of the nth mode and $I_{dd}(\omega)$ describes the frequency content of the disturbance. The asterisk denotes the complex conjugate of the transfer function output. Again assuming a disturbance composed of white noise results in

$$\langle \Pi \rangle = \frac{1}{2} \sum_{n=1}^{N} \Re \{ H_{dQ}(\omega) H_{d\dot{q}}^{*}(\omega) \}. \qquad (2\text{-}81)$$

Radiation Resistance and Radiation Efficiency

Radiation resistance is the real part of the radiation impedance of a structure. This quantity can be defined as[9]

$$R_{n} = \frac{\langle \Pi_{n} \rangle}{\langle |\dot{q}_{n}|^{2} \rangle} . \qquad (2\text{-}82)$$

Normalizing Equation (2-82) by the characteristic impedance of the fluid medium and the area radiating, yields the relationship for radiation efficiency or radiation ratio,

$$\sigma_{n} = \frac{\langle \Pi_{n} \rangle}{\rho c a b \langle |\dot{q}_{n}|^{2} \rangle}. \qquad (2\text{-}83)$$

The state variable structure of the system model can also yield a transfer function between the nth input generalized force and the nth output generalized velocity. This relationship can be written as

$$\tilde{Q}_n e^{j\omega t} = H_{Q\dot{q}}(\omega)\tilde{\dot{q}}_n e^{j\omega t}.$$ (2-84)

Substituting Equation (2-84) into Equation (2-75) results in

$$\Pi_n(t) = \Re\{H_{Q\dot{q}}(\omega)\}(\tilde{\dot{q}}_n e^{j\omega t})^2.$$ (2-85)

Taking the time average of this relationship yields

$$\langle\Pi_n\rangle = \frac{1}{T}\int_0^T \Re\{H_{Q\dot{q}}(\omega)\}(\tilde{\dot{q}}_n e^{j\omega t})^2 dt = \frac{1}{2}\Re\{H_{Q\dot{q}}(\omega)\}\tilde{\dot{q}}_n^2,$$ (2-86)

when combined with Equation(2-61), this allows Equation (2-74) to be rewritten as

$$\sigma_n = \frac{4\Re\{H_{Q\dot{q}}(\omega)\}}{\rho cab}.$$ (2-87)

Validation of the Model and the Method

This modeling method has been validated in previous work by Frampton[5,13]. This work showed that the radiation efficiency curves published by Wallace[9] are reproduced using the state variable, coupled aerodynamic / structural model derived in the previous section with the transfer function expressions for radiation efficiency. Similarly, the model reproduces the curves for convected flow that were published by Graham[4]. In this work, supersonic convection velocities will be used with the previously defined relationships describing kinetic energy and radiated power.

It must be noted that the use of linearized potential flow (Equation 2-33) is known to be inaccurate in the transonic region. Nonlinearities in the fluid dynamics become

significant and should be accounted for. However, there are some interesting and instructive conclusions to be drawn from this linear model. The establishment of more accurate, nonlinear results is left for future work.

The radiation efficiency is evaluated using non-dimensional frequency, defined as

$$\gamma = \frac{k}{\sqrt{\left(\dfrac{m\pi}{a}\right)^2 + \left(\dfrac{n\pi}{b}\right)^2}} \qquad (2\text{-}88)$$

where k is the acoustic wave number, given by:

$$k = \frac{\omega}{c}. \qquad (2\text{-}89)$$
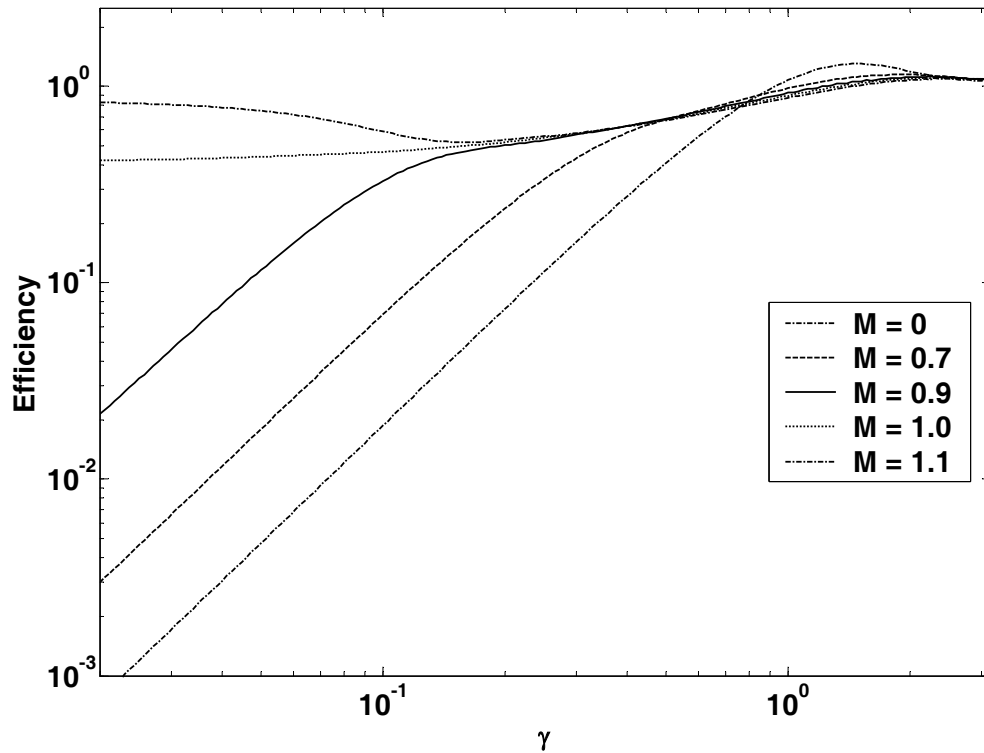
Figure 2-6.   Radiation efficiency of the (1, 1) mode at selected flow velocities

31

Figure 2-6 shows the behavior of the radiation efficiency of the (1, 1) mode at transonic speeds and at two subsonic speeds. Note that the radiation efficiency for $M = 0$ compares well with that found by Wallace[9], and the $M = 0.7$ case compares well with that noted by Frampton[5]. In general, the radiation efficiency approaches a magnitude of unity for all frequencies as the speed of sound in the medium is exceeded.
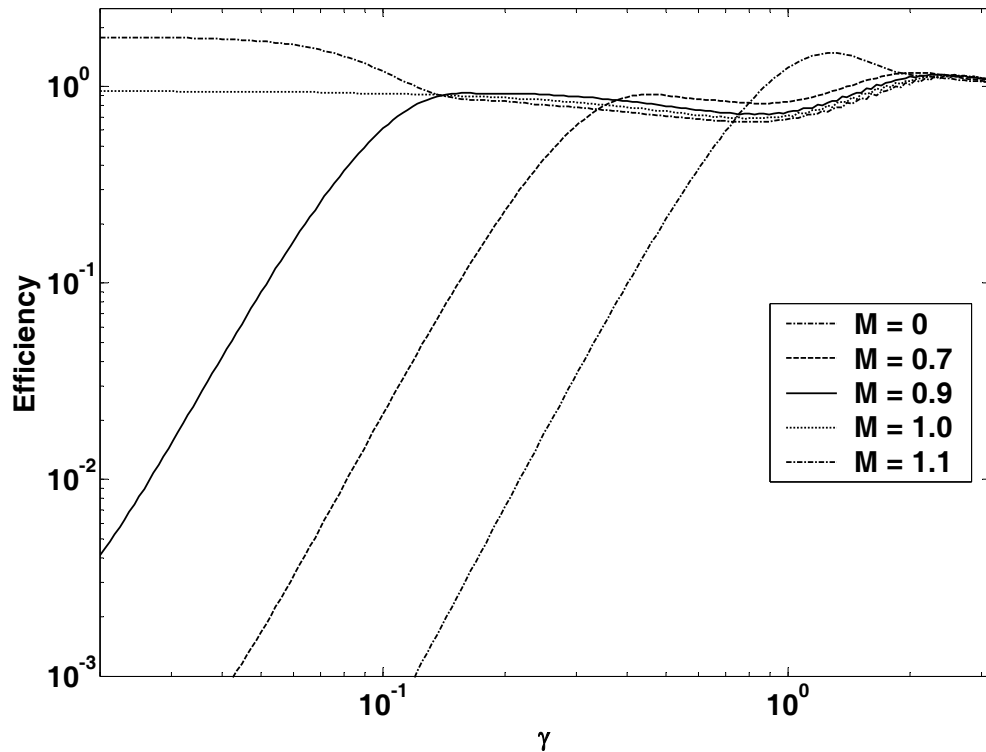
Figure 2-7.   Radiation efficiency of the (2, 1) mode at selected flow velocities

Figure 2-7 shows the behavior for the (2, 1) mode. Again, the low frequency radiation efficiency increases significantly when the Mach number approaches unity.

Increases in radiation efficiency of *in vacuuo* modes without coupling were dealt with previously[5]. The cause of this increase in radiation efficiency was found to be an effective increase in plate phase velocity for plate waves traveling upstream relative to the flow. Furthermore, the radiating wave number region broadens as flow velocity increases, reaching an infinite width as Mach number approaches 1. In the simplified case of a 1-dimensional plate the radiating wave number region is defined as the region in which the z-component of the wave numbers are real and positive[5]. This corresponds to

$$\left(\frac{k_z}{k}\right)^2 = 1 - 2M\left(\frac{k_x}{k}\right) + \left(M^2 - 1\right)\left(\frac{k_x}{k}\right)^2 . \tag{2-90}$$

As demonstrated in Equation (2-90), the supersonic wave number region shifts and expands as Mach number increases and becoming (semi-)infinitely wide when $M = 1$. The overall effect in subsonic flow is that, for a fixed wave number spectrum in the plate response, as the flow velocity increases more of the plate wave number spectrum is enveloped by the radiating region, thus resulting in increased radiation.

When flow becomes supersonic, the non-radiating region shifts to wave number ratios that are strictly positive. Figure 2-8 demonstrates this phenomenon. Equation (2-90) is a description of the roots of

$$0 < 1 - 2M\left(\frac{k_x}{k}\right) + \left(M^2 - 1\right)\left(\frac{k_x}{k}\right)^2 , \tag{2-91}$$

where k_z is the wave number component in the convected fluid normal to the plate, k_x is the wave number in the plate, and k is the wave number in the fluid. In order for radiation to take place,

$$\frac{k}{M-1} < k_x < \frac{k}{M+1} \tag{2-92}$$

33

Figure 2-8 shows a plot of this equation for a semi-infinite plate, where the plate is bounded in the *x* direction and unbounded in *y*. The cases where $M = 0$ (no flow), $M = 0.8$, $M = 1.0$ and $M = 1.3$ are shown. The labeled vertical bars indicate the boundaries of the radiating wave number regions. Note that the radiating regions are shifted due to the effect of the flow speed on the relationship between the wave number in the plate and the wave number in the fluid. Also note that for $M = 1.3$ the radiating region is again affected by the flow. All waves traveling against the flow of the fluid radiate to the far field. In addition some slower wave numbers that travel in the direction of the flow radiate as well. While these wave numbers are not supersonic alone, the speed of the flow makes them appear supersonic to the fluid. The faster wave numbers also radiate as one would expect.
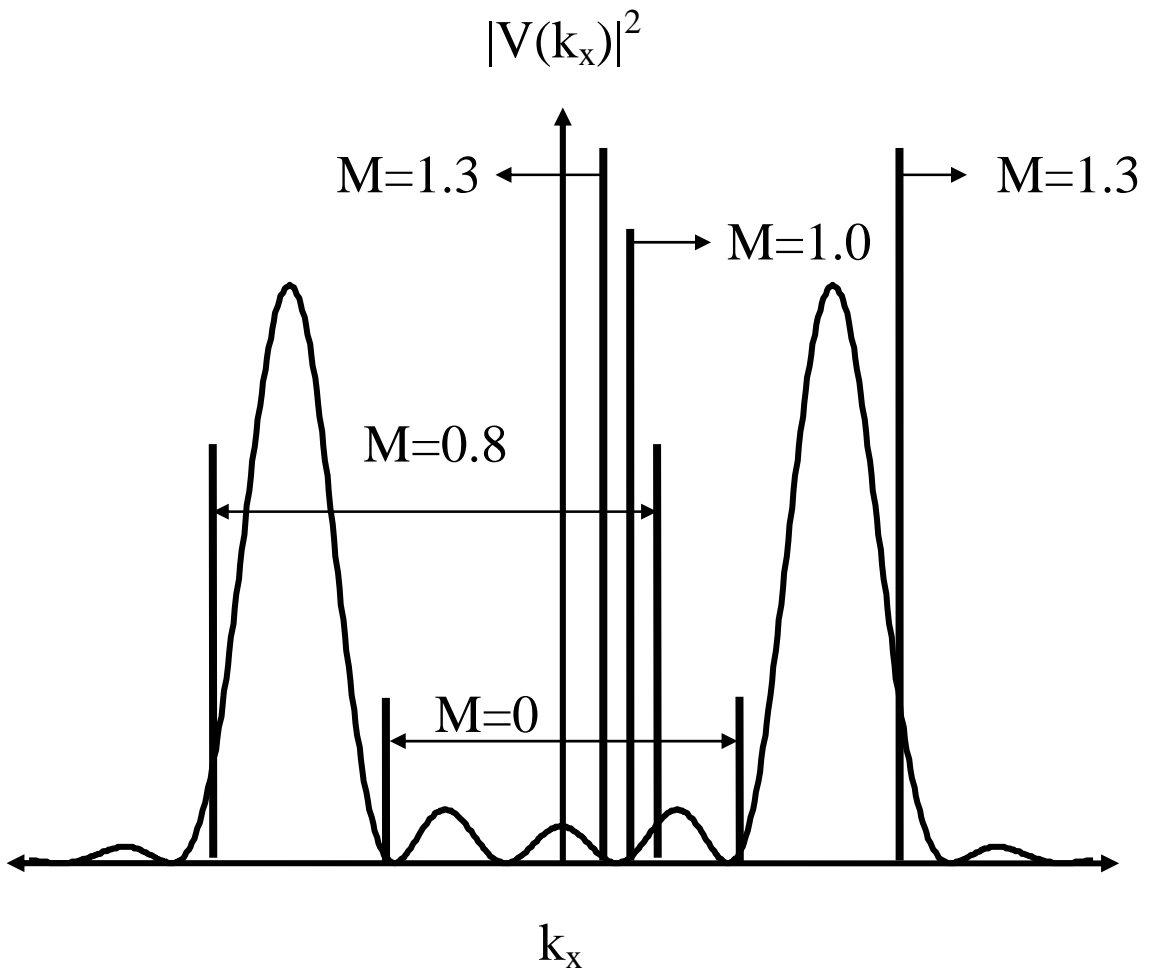
Figure 2-8. Plot of the wave number spectrum of plate velocity showing the radiating portions for selected Mach numbers

CHAPTER III

SIMULATION RESULTS

Physical System Parameters

A computational investigation was undertaken based on the theory presented in Chapter II. The results presented focus on three areas: the behavior of the uncoupled modal radiation efficiency at transonic flow speeds, the effects of flow-induced coupling on the structural response and on the radiated sound power. The physical parameters used were for a plate manufactured from 6061-T6 (UNS A96061) aluminum (density of 2700 kg/m^3, thickness of 4 mm, length of 1 m in the direction of flow, width of 0.83 m and modulus of elasticity of 69 GPa) exposed to air at an altitude of 10 km (density of 0.422 kg/m^3, speed of sound of 299.5 m/s). A constant modal damping ratio of 2% was assumed in the formulation of the plate model.

The accuracy of the modeling approach used in this work was established previously[13], where results for the subsonic case were presented. In order to ensure accurate results, the plate model of Equation (2-14) included 20 modes while the fluid dynamic system of Equations (2-62) – (2-65) included 600 degrees of freedom. With this configuration, the plate response and radiated sound power demonstrated sufficient convergence over the first 15 plate modes.

Supersonic Flow

Structural Response

It is well established that fluid flow can have significant effects on structural acoustic behavior, along with the fact that induced coupling between discrete modes of vibration becomes significant as flow velocity increases. It has also been established that this coupling mechanism is the venue for energy flow between distinct modes of vibration in a structure, explaining energy flow into the flowing fluid. Work in this area has been confined to subsonic flows, with the effect on sound radiation efficiency and sound power radiation quantified and compared for various subsonic flow speeds.

The effect of flow on plate dynamics is well understood in the field of aeroelasticity[10]. However, this field of study is usually concerned with coupling induced instabilities. These instabilities are not usually of interest in structural acoustics since structures being investigated are designed to avoid them. However, the effects on plate dynamics can occur when the structure is far from instability, therefore affecting structural acoustic behavior. In the structural acoustics literature Sgard, Attalla and Nicolas[11] quantified modal coupling with an approach based on the coherence between modes.

The results of this work showed some interesting behavior when compared to earlier work done for subsonic flow speeds. Supersonic flow velocities produced structural response variations similar to those produced by subsonic flow, but exhibited a frequency shift proportional to flow speed, rather than the inverse relationship observed for subsonic flow speeds.

The effect of flow on the structural response is demonstrated in Figure 3-1 which shows the frequency dependent kinetic energy of the plate for one subsonic and various supersonic flow velocities. A general upward shift in fundamental mode frequency is observed as the Mach number increases. The resonant frequencies of the coupled modes do not change considerably as the Mach number increases above a value of 1.2. The fundamental coupled mode has a resonant frequency of about 18 Hz when $M = 1.2$ moving to 25 Hz when $M = 2.0$.

Other modes show small changes in frequency and response amplitude as well. However, other than the fundamental mode frequency shift, the plate energy changes very little with increasing supersonic Mach number.
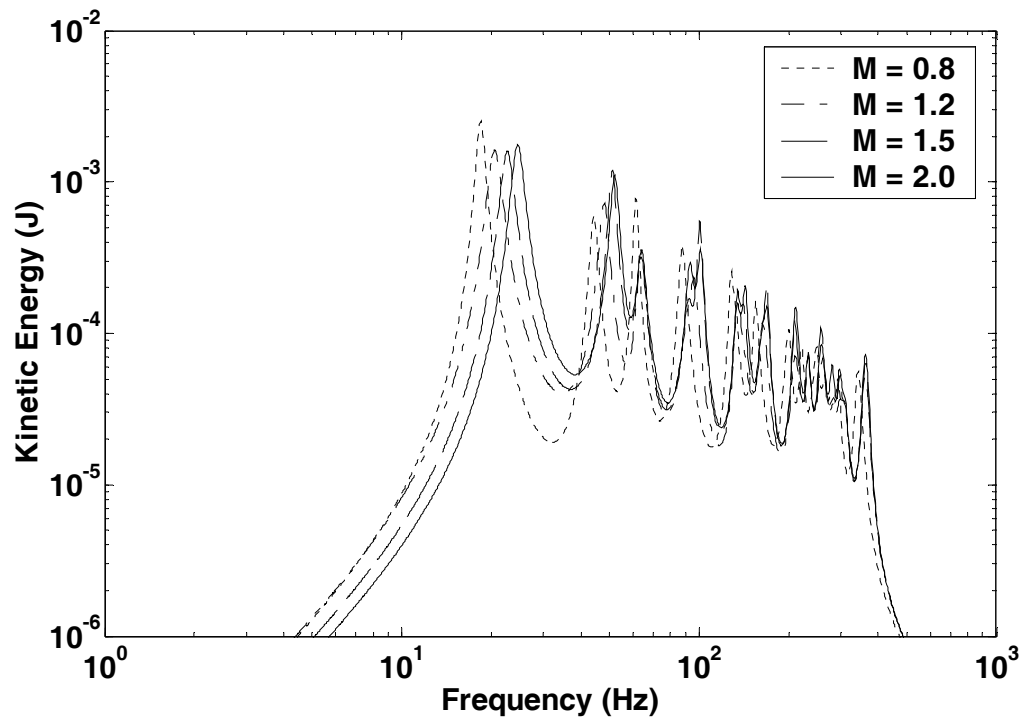
Figure 3-1.   Structural kinetic energy in supersonic flow

Radiated Sound Power

Supersonic flow also had a significant effect on power flow in the structure, with some modes containing significant negative components at low supersonic flow velocity and with the entire structure exhibiting a negative net power flow at the higher supersonic speeds considered.

The effect of aerodynamic flow on the radiated power in the plate is shown in Figure 3-2, which shows the radiated sound power as a function of frequency for one subsonic 3-2(a) and several supersonic Mach numbers 3-2(b) – 3-2(d).
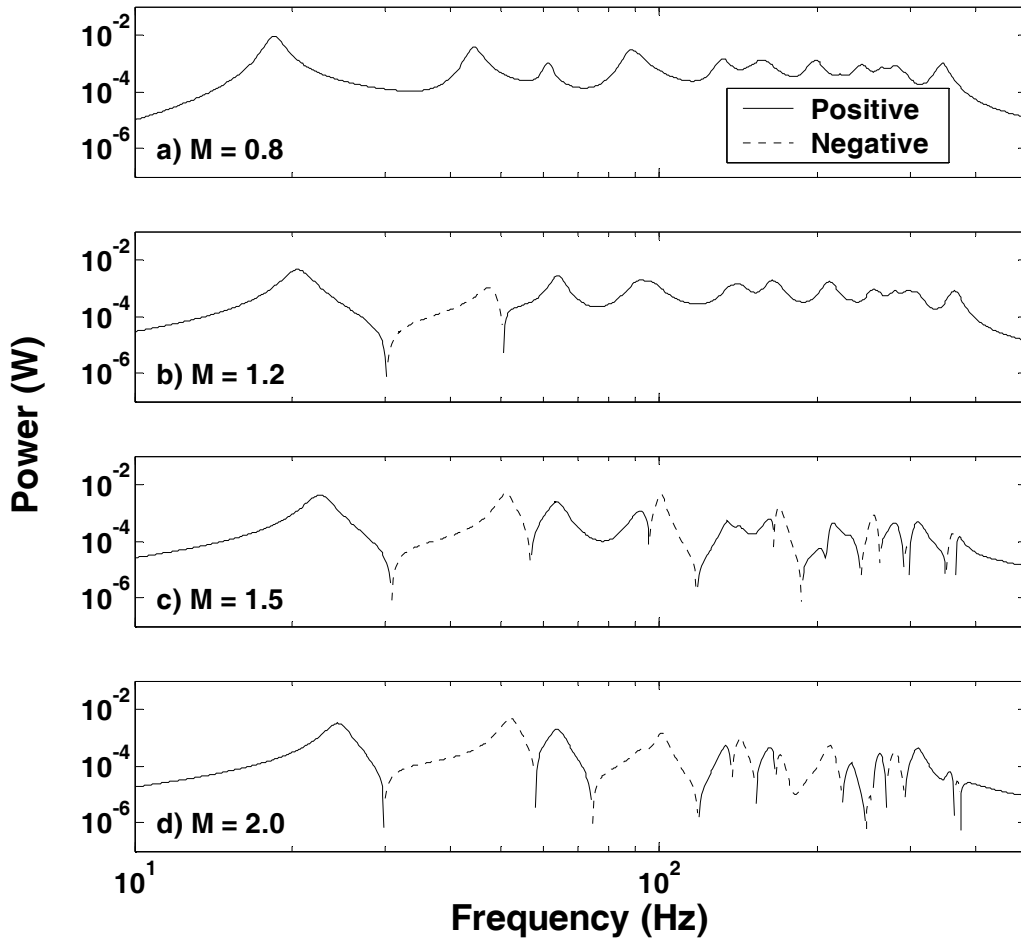
Figure 3-2.   Radiated sound power in supersonic flow

Note that, while the kinetic energy changed little over the range of supersonic flows, the radiated power curves do change significantly. Overall, the radiated power decreases with increasing flow speed. As convection velocity increases, significant portions of the power flow curve become negative. This behavior indicates energy absorption by the structure rather than radiation. This is a very interesting aspect of the redistribution of energy through flow-induced modal coupling. The path through which

energy moves from one coupled structural mode to another is the fluid. In this manner the

motion of one mode drives other modes, causing them to be out of phase with the

pressure applied by the aerodynamics, resulting in negative power flow at some

frequencies. This energy is then dissipated by damping in the plate.
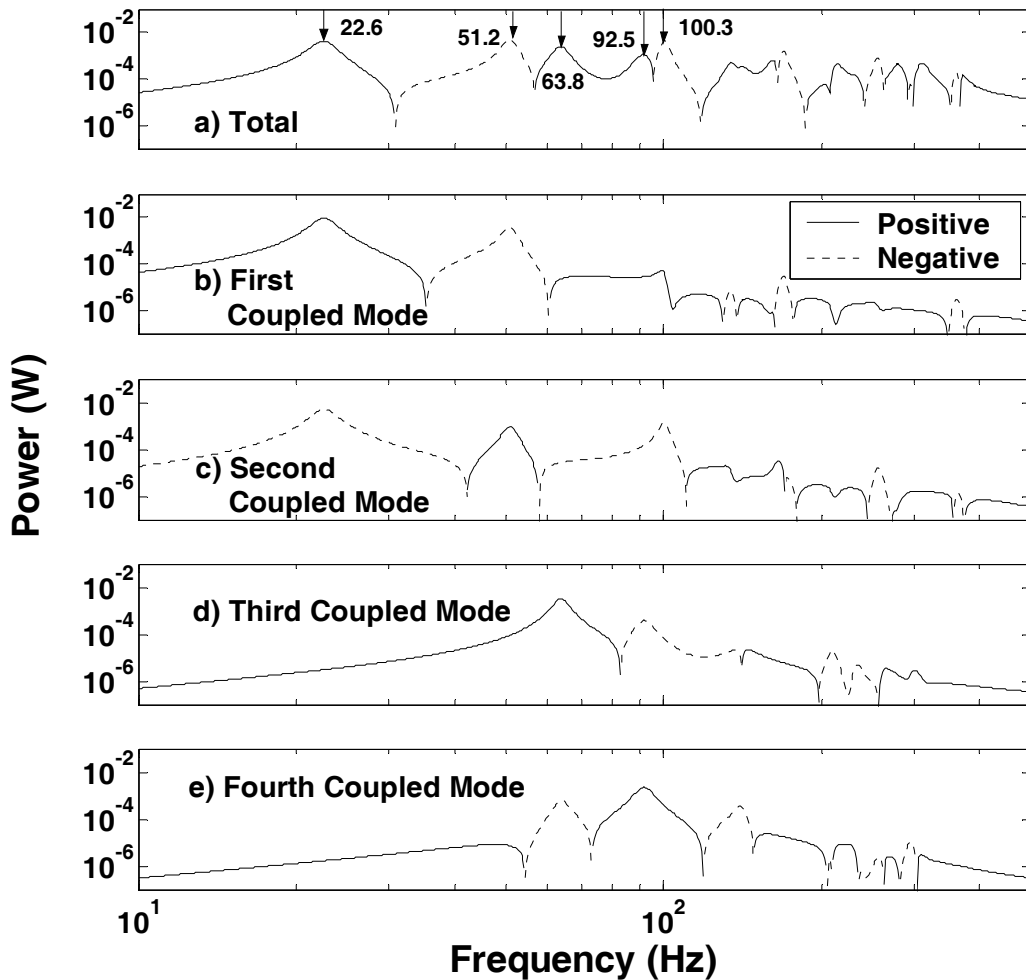
Figure 3-3.   Modal contributions to radiated sound power at *M* = 1.5

Figure 3-3 illustrates this behavior by plotting the total power flow at a selected velocity 3-3(a) with the contributions of the first four coupled modes also plotted individually 3-3(b) – 3-3(e). Subplot 3-3(a) also lists the peak frequencies on the kinetic energy plot (Figure 3-1) attributable to the associated uncoupled modes for reference.

Clearly, the exchange of energy among modes that occurs in the presence of modal coupling alters not only the dynamic response of the plate but the radiated sound as well. The extent to which coupling affects radiation is demonstrated by the curve for $M = 2.0$ in Figure 3-2. Many higher order modes absorb power, causing the total power radiated to the far field to decrease as flow speed rises. Radiated power decreases, and actually becomes negative (i.e., net power is absorbed) as the flow speed approaches Mach 2.

Radiation Efficiency

The effect of modal coupling is also illustrated in Figure 3-4, which plots the total normalized power flow versus flow velocity. Radiation efficiency for a single mode of vibration as a function of frequency is described by Equation (2-87). The data shown in Figure 3-4 are given by

$$\sigma_T = \sum_{n=1}^{N} \int_0^{\omega_{max}} \sigma_n \, d\omega. \tag{3-1}$$

This quantity, which can be visualized as the energy flow out of the plate divided by the total kinetic energy from vibration, is considered the total radiation efficiency here.
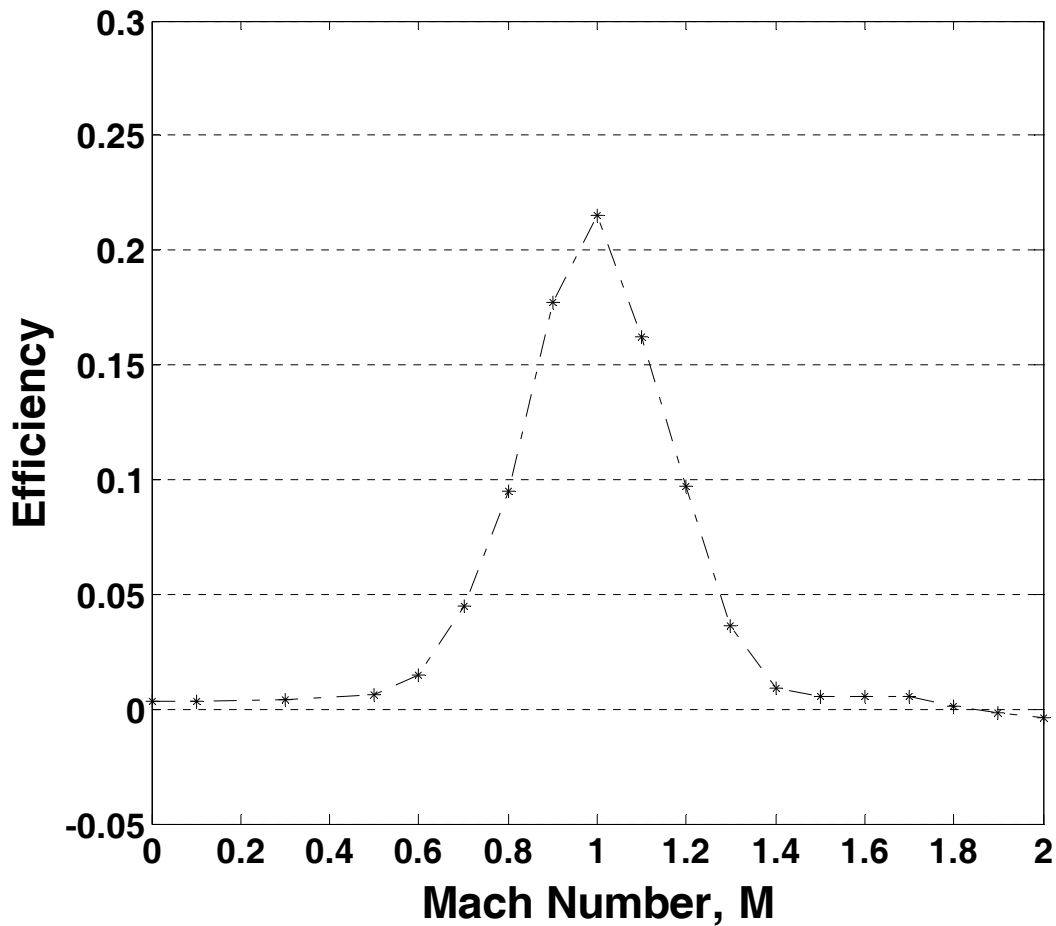
Figure 3-4.   Total radiation efficiency in supersonic flow

The total radiation efficiency obtained for the range of flow speeds studied expands those

found in previous work. Rather than increasing with flow speed as previously postulated,

the radiation efficiency rises with subsonic flow velocity. Total radiation efficiency

peaks at $M = 1.0$ as predicted, and decays with further increases in flow speed. It should

be noted that the radiation efficiency decays to a negative value with the radiated power

as convection velocity increases. This behavior illustrates the role of coupling on power

flow at high convection velocities. This result provides further insight into the dynamics

of power flow in the structure and may indicate a relationship between acoustic power radiation and the onset of instability of the structure. Further work is needed to establish the existence of any meaningful connection between these two phenomena.

Effects of In-plane Stress

The significant impact of coupled fluid flow on structural acoustic behavior established by previous work has been confined to flow in air, over unloaded structures, with the effects on sound radiation efficiency, kinetic energy and sound power radiation quantified and compared for various flow speeds.

The plate system was investigated for values of non-dimensional stress, defined as[19]:

$$r = \frac{N_x a^2}{\pi^2 D} \tag{3-2}$$

ranging from -2 to 20. This group of plate models was coupled with aerodynamic models that represented speeds from Mach 0.001 up to Mach 2.0. The values of non-dimensional stress were the same in both the x and y directions. These limits were chosen to represent the lower end of static stability of the plate ($r = -2$) and a stress state that would be typical of the skin of an aircraft structure when in flight ($r = 20$). The uncoupled plate system was found to be statically unstable when r was set to a value of -2.5 at flow speeds between Mach 0.8 and Mach 1.2. Each coupled system was checked for dynamic instability, and all systems investigated were found to be stable, with the exception of the cases noted above.

Structural Response with In-plane Stress

The overall effect of flow on the structural response is demonstrated in Figures 3-5 and 3-6, which show the frequency dependent kinetic energy of the plate for various subsonic and supersonic flow velocities, with several selected values of non-dimensional stress.

Initially, the structure was examined when placed in a biaxial state of stress. That is, both the *x* and *y* directions in the plane of the plate had equivalent values of non-dimensional stress. The structural response of the system is similar to what would be expected based on earlier work with unloaded structures in subsonic flow[5,13]. As subsonic flow speeds increase, the response frequency of the fundamental mode of vibration decreases. This behavior is affected by the state of stress in the structure, however. When the overall state of stress is compressive, as shown in Figure 3-5a, the shift in fundamental mode response frequency is most pronounced.

Behavior at supersonic flow speeds also is as expected based on work in the previous section. As supersonic flow speed is increased, response frequency of the fundamental mode of vibration also increases. Again, the frequency shift of the structure when loaded in compression shows the largest frequency shift in fundamental mode response with variations in flow velocity, as shown in Figure 3-6a.

45
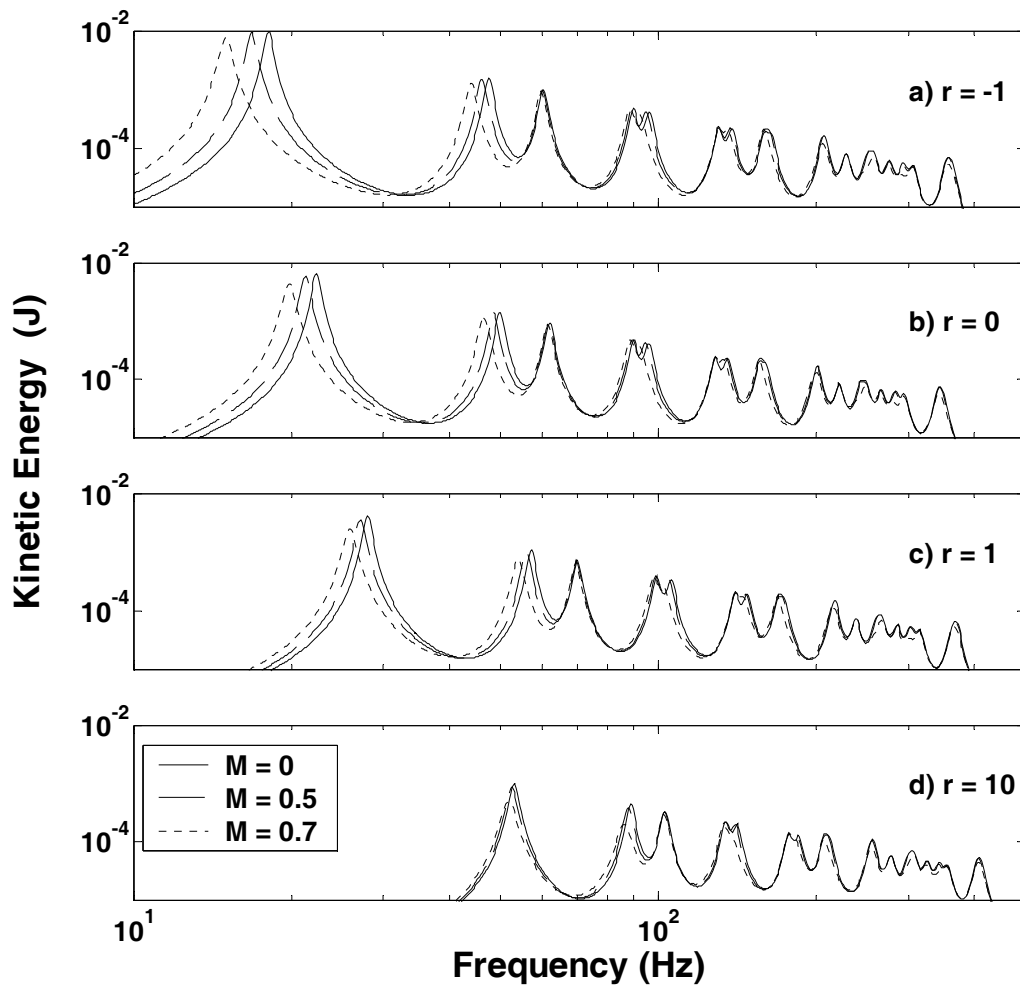
Figure 3-5.   Structural kinetic energy at subsonic convection velocities for selected
values of non-dimensional stress

A general upward shift in coupled mode frequency is observed as the non-dimensional stress in the plate rises, as one would expect from an effective increase in plate stiffness
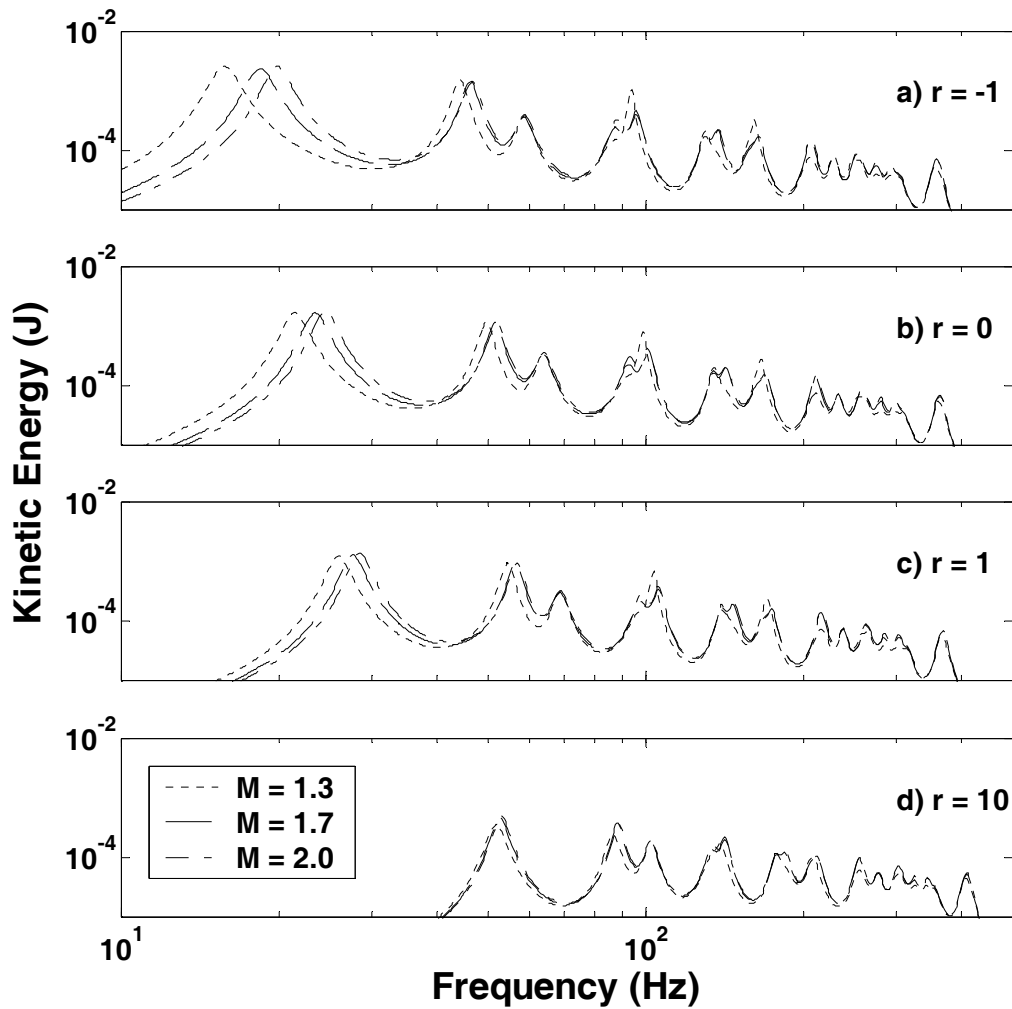
Figure 3-6.   Structural kinetic energy at supersonic convection velocities for selected values of non-dimensional stress

It is also important to note that the total kinetic energy of the plate decreases as non-dimensional stress is increased, but does not vary greatly as convection velocity is increased. It should also be noted that the frequency shifts observed are attributable to convection effects. While the level of applied stress changes the way these frequency

shifts manifest themselves, application of stress in and of itself will not produce similar effects.

Radiated Sound Power with In-plane Stress

The effect of aerodynamic flow on the radiated power from the plate is shown in Figures 3-7 through 3-10, which show the radiated sound power as a function of frequency for various subsonic and several supersonic Mach numbers at selected values of non-dimensional stress. The effect of in-plane stress on radiated sound is greatly affected by the proximity to the system stability boundaries. When the stress is compressive, and the uncoupled plate system is close to it's static stability boundary (i.e., near buckling), the radiated power is increased over what would be obtained from a plate with no imposed stress or with imposed tensile stress. This is best illustrated by comparing Figures 3-7c, 3-8c and 3-9c, and noting the decreasing area under the power curve.

When the coupled system is approaching the flutter boundary (as flow approaches Mach 2), the total radiated power can actually become negative, indicating a net absorption of power by the structure, as shown in Figures 3-9f and 3-10f.

The power flow in the structure is also significantly affected by the state of stress in the structure. When the stress in the structure is compressive, there is an increase in the amount of negative power flow at high convection velocities. The amount of energy absorbed by the second mode of vibration can be seen to steadily decrease as the state of stress moves from compression to zero stress to tension, as shown in Figures 3-7f, 3-8f, 3-9f and 3-10f, for example. The number of modes of vibration having negative power

48

contributions decreases from 9 to 6 over this same progression of states of stress, and shown in these same figures. The transition to higher levels of tensile stress also delays the onset of negative power contributions of particular modes of vibration as a function of flow velocity. This behavior is illustrated in Figures 3-7d, 3-8d, 3-9d and 3-10d. The 2nd, 5th and 8th modes of vibration show a negative power flow until the highest state of stress studied is reached in Figure 3-10.

Note that, while the general shapes of the kinetic energy curves change little over the range of values of non-dimensional stress, the radiated power curves do change significantly. Overall, the radiated power decreases as flow speed increases or decreases from Mach = 1.
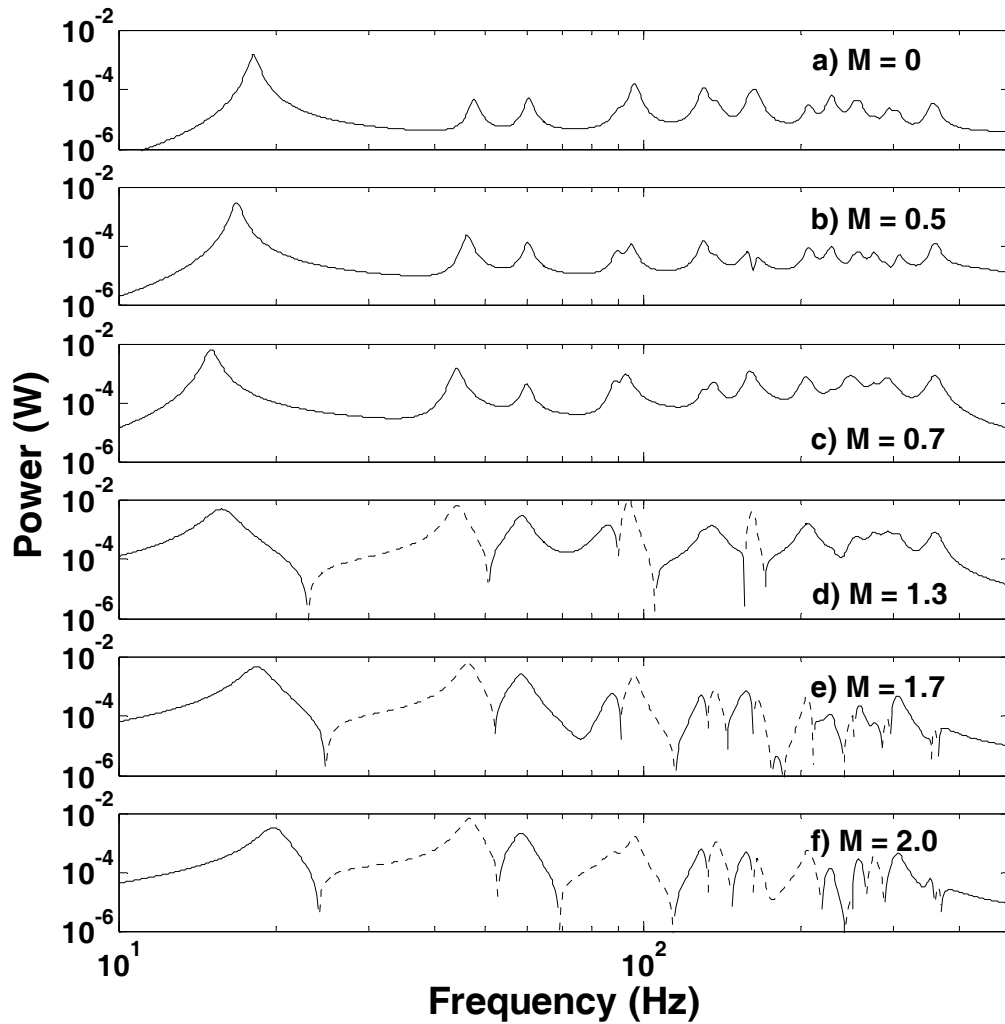
Figure 3-7.   Radiated sound power for $r = -1$ at selected convection velocities

Once again, note that as supersonic convection velocity increases, significant portions of the power flow curve become negative. This behavior changes significantly when the state of stress in the structure is varied. This indicates that the state of stress in the structure affects the redistribution of energy caused by flow-induced modal coupling.
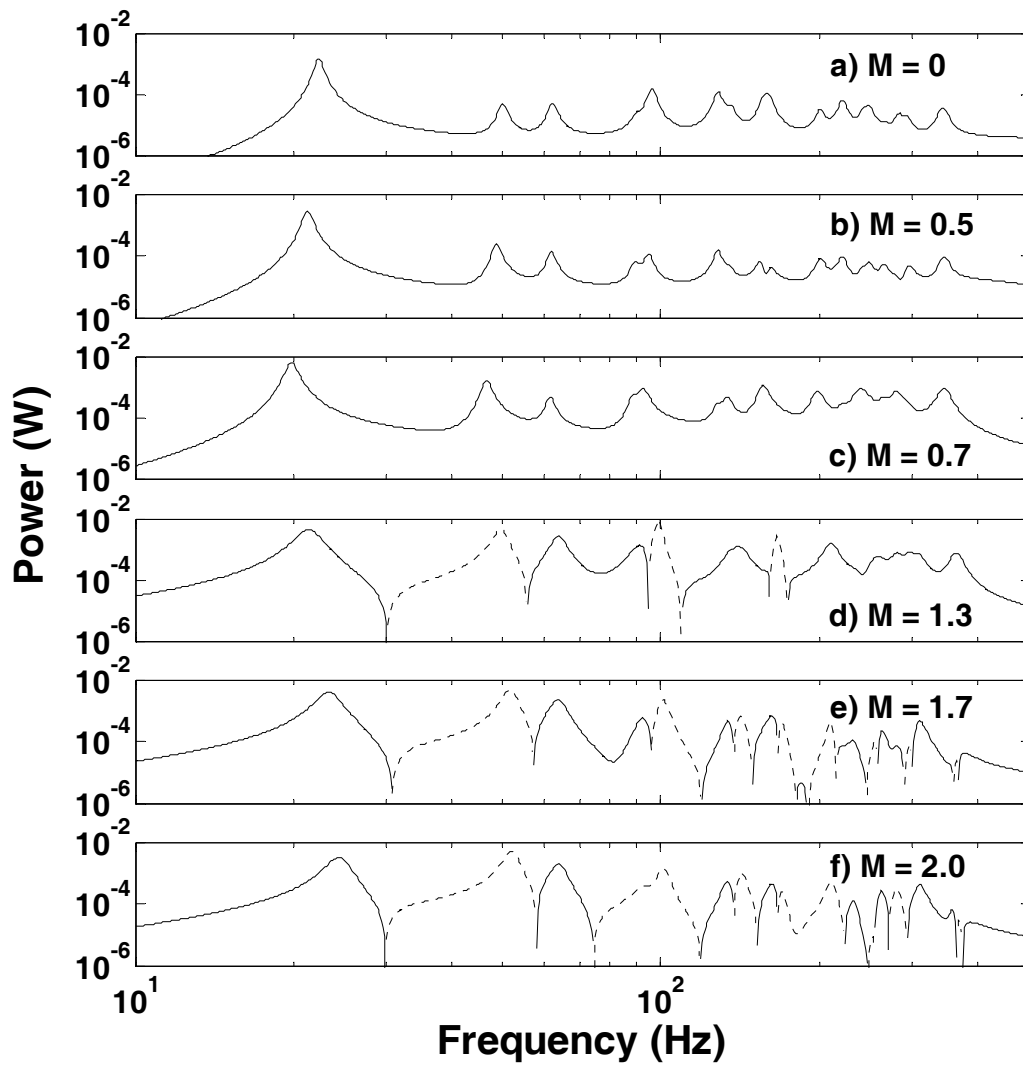
Figure 3-8.   Radiated sound power for $r = 0$ at selected convection velocities
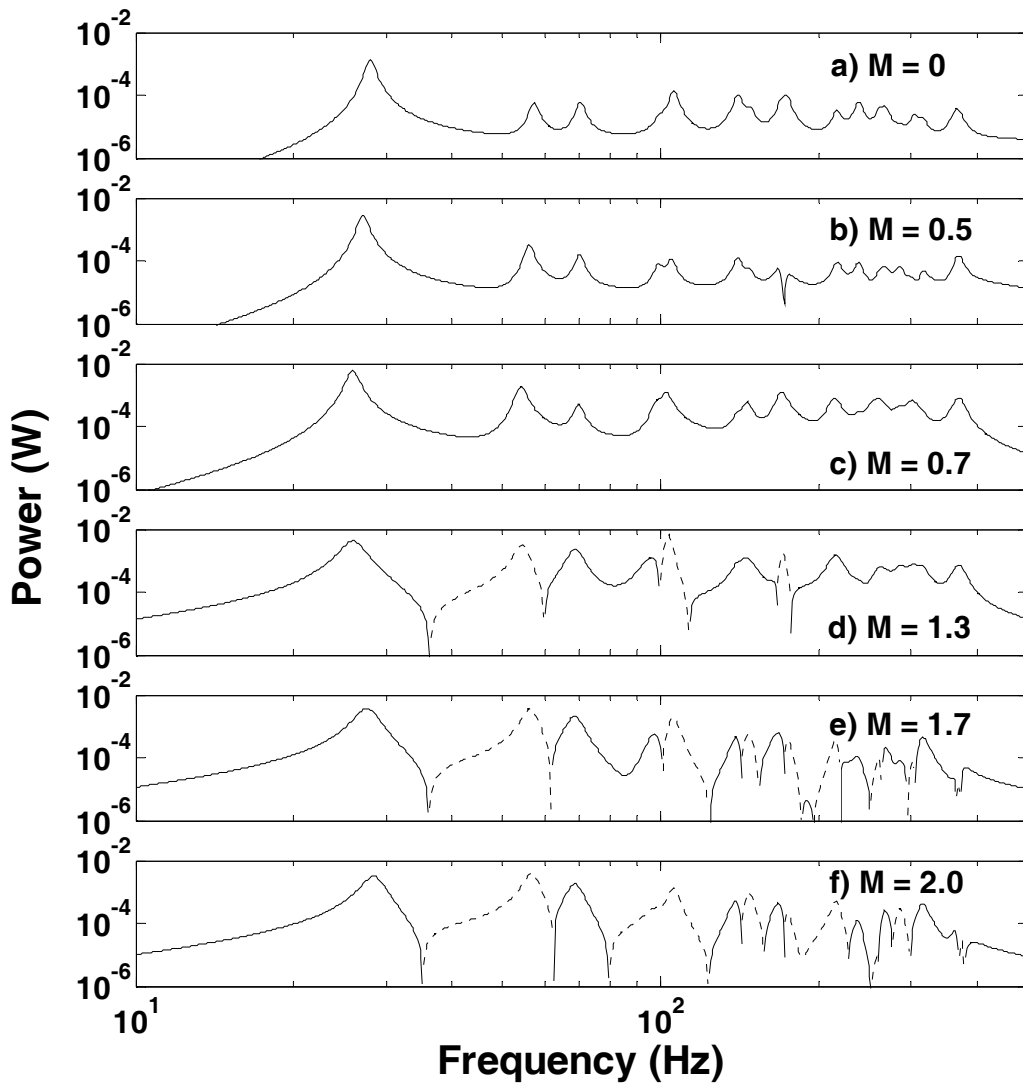
Figure 3-9. Radiated sound power for $r = 1$ at selected convection velocities

The extent to which coupling affects radiation is demonstrated by the curves for the data at higher Mach numbers. Many higher order modes absorb power, causing the total power radiated to the far field to decrease as flow speed rises.
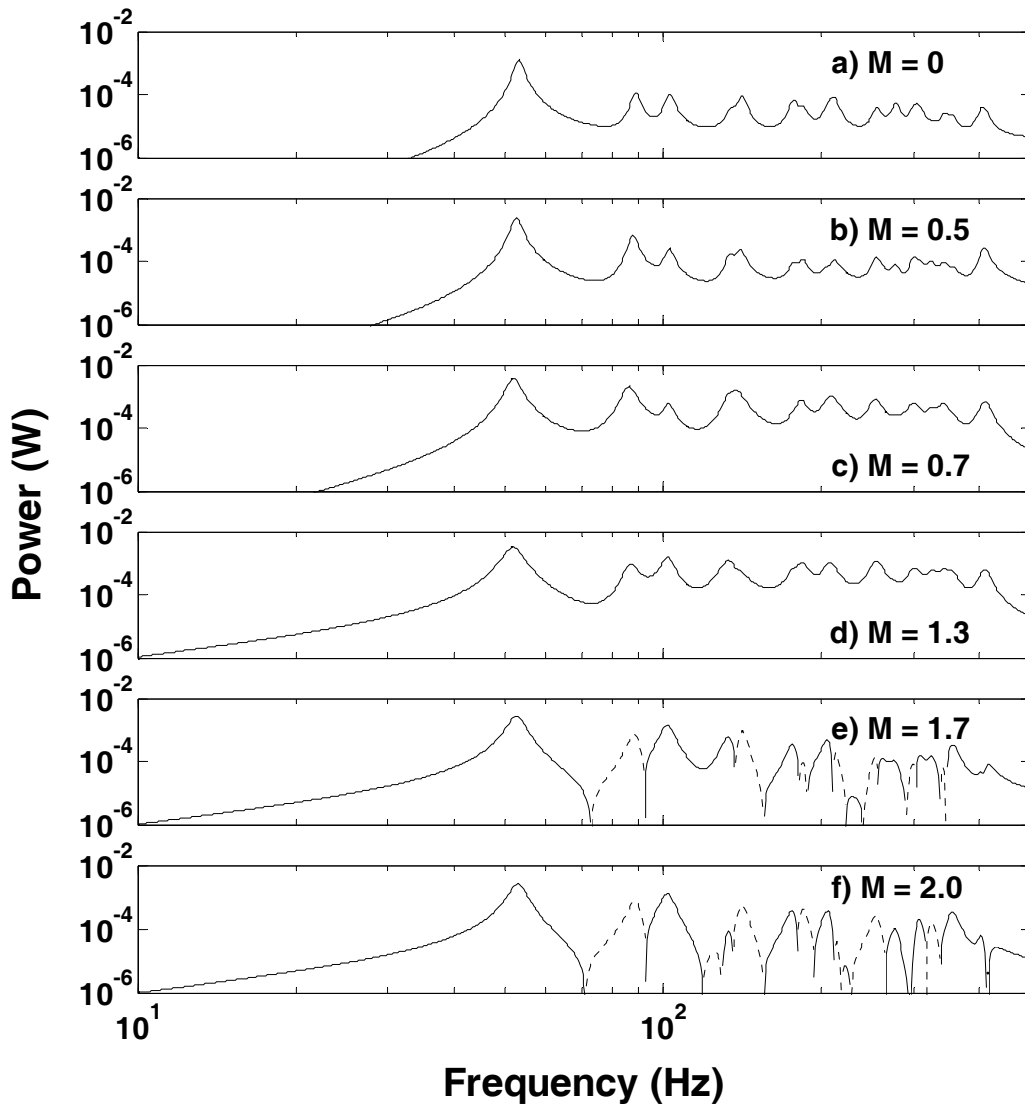
Figure 3-10. Radiated sound power for *r* = 10 at selected convection velocities

Radiated Sound Power with Unidirectional In-Plane Stress

In addition to varying the levels of stress in the plate, the effects of the direction

of application of the stress were studied. Simulations with stress applied only in the *x*

and only in the *y* direction were examined. Figures 3-11 and 3-12 show the results for

two of these unidirectional stress cases. Application of stress in the direction of flow results in increased negative power flow at higher frequencies and at high convection velocities, as shown in Figure 3-11.
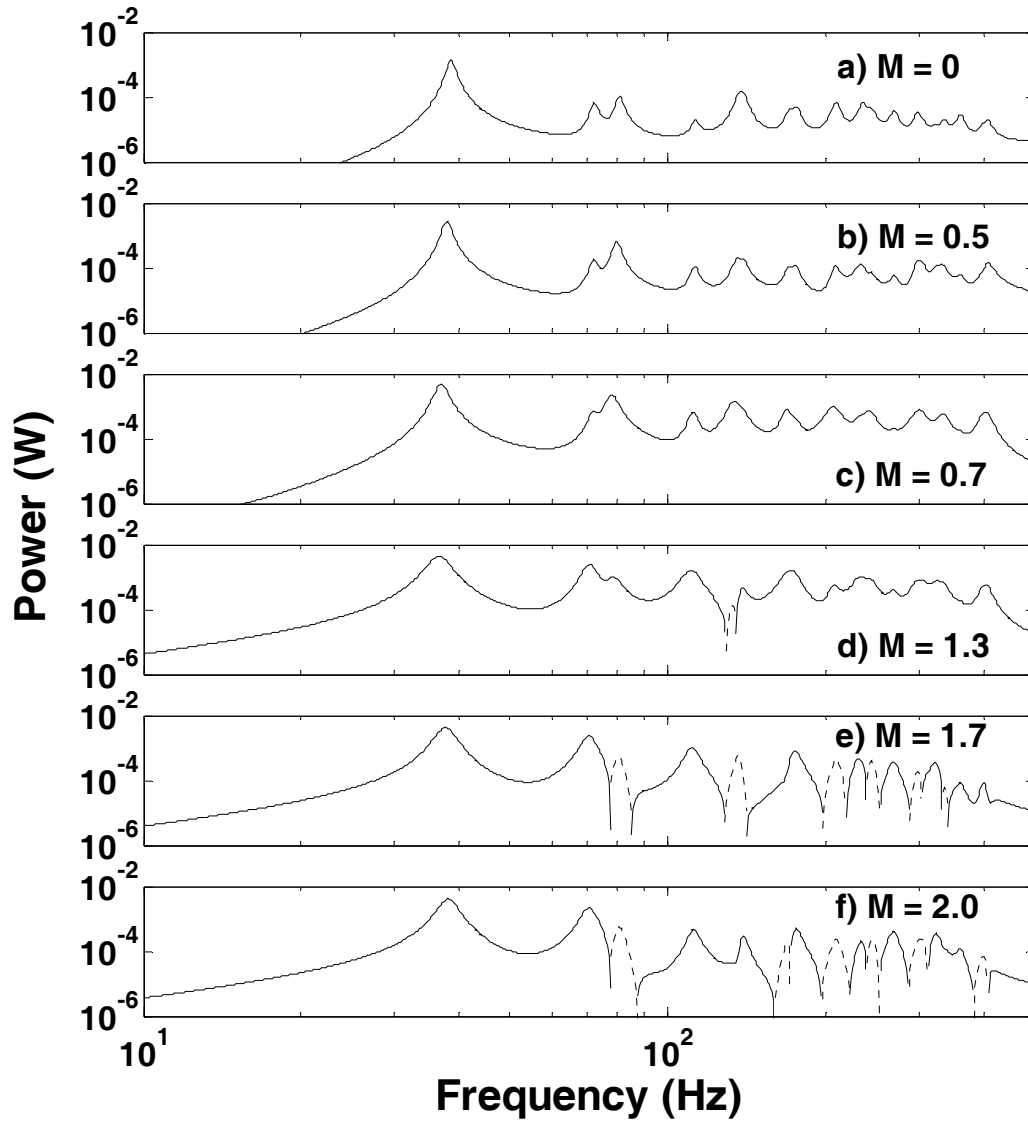
Figure 3-11.   Radiated sound power for $r = 10$, stress applied in the x direction only at selected convection velocities

Figure 3-12 shows the application of stress perpendicular to the convection velocity (i.e., the *y* direction in Figure 2-1) results in less power radiated by the fundamental mode as convection velocity increases. Unidirectional stresses in these cases resulted in lower resonance frequencies for the fundamental modes than shown for the case with bidirectional stress, as shown for example in Figures 3-8a, 3-9a and 3-10a.
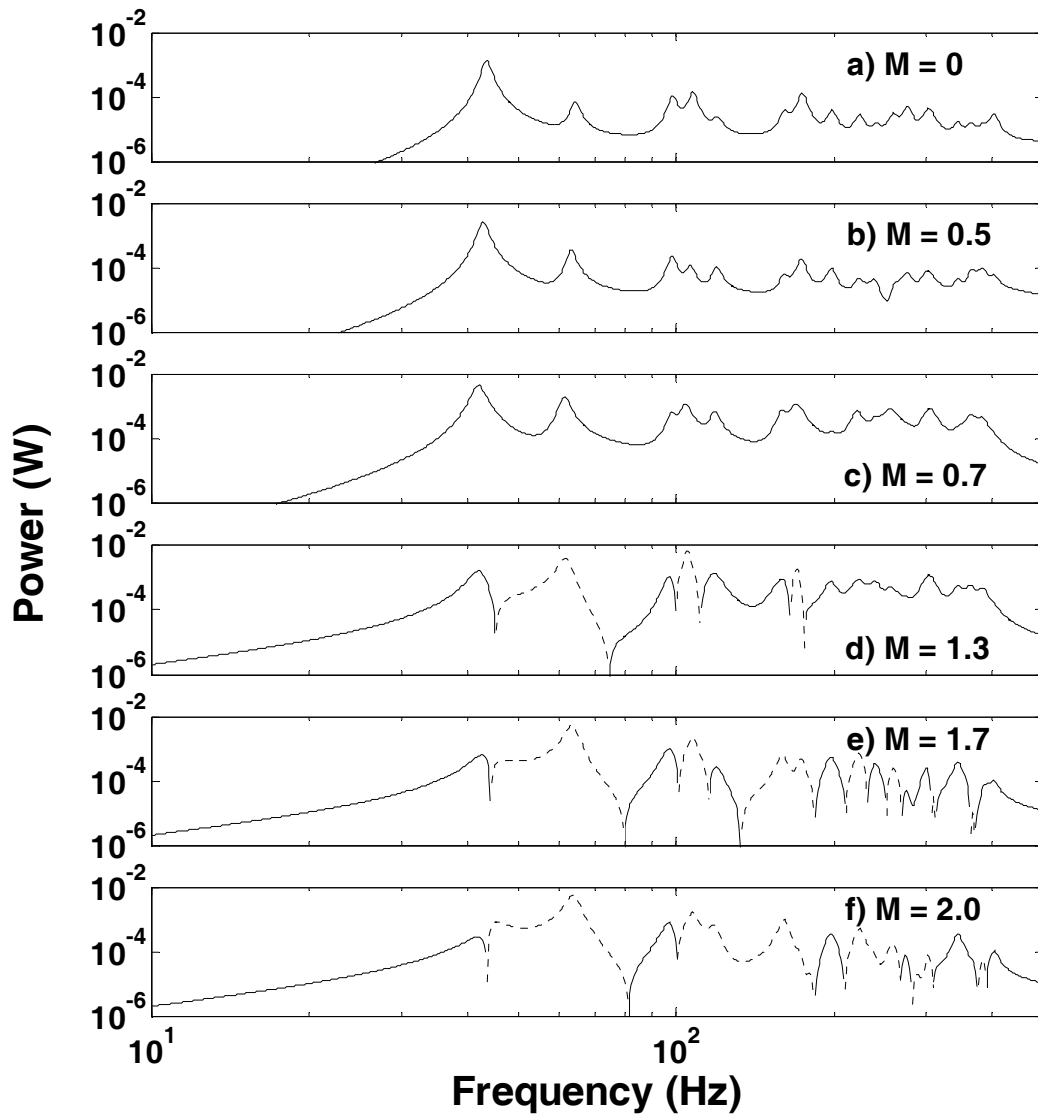
Figure 3-12.   Radiated sound power for $r = 10$, stress applied in the y direction only at selected convection velocities

The frequency shifts in these cases were observed to be different, as would be expected from an overall lowering of the state of stress in the structure. Differences in the power flow characteristics of individual coupled modes of vibration were observed. When stress is applied only in the x direction, which is also the direction of fluid flow,

the power flow in the 2nd coupled mode of vibration is positive for all convection velocities studied, as shown in Figure 3-11. Very little negative power flow is induced in the structure, even at high convection velocities. When stress is applied only in the *y* direction (perpendicular to the direction of flow) both the 2nd and 3rd coupled modes exhibit significant negative power flow, as shown in Figure 3-12. It is also interesting to note the significant decrease in response of the fundamental coupled mode with increase in flow velocity. The power associated with this mode is attenuated by about an order of magnitude over the range of flow speeds studied.

This effect is strictly due to the reduced overall applied stress and is not attributable to convection effects. It is interesting to note that the reduction in fundamental resonance frequency is greater in the case where the stress is applied in the direction of convection, which is attributable to structural interaction with the flow. Similar effects were noted for cases with reduced stress levels($r = 0$, $r = 1$), but were not as prevalent as those illustrated in Figures 3-11 and 3-12.

Radiation Efficiency with In-plane Stress

As discussed previously, the linearized potential flow relationship shown in Equation (2-23) is known to be inaccurate for convection velocities around Mach = 1. Nonlinearities in the fluid dynamics are present and should be considered. The linear model is useful in studying general trends of fluid behavior, even if numerical results can not be considered exact. With these limitations in mind, the linear model will be used to generate a continuous curve for radiation efficiency for structures with imposed stress.

Figure 3-13 shows a plot of total radiation efficiency versus convection velocity for selected values of non-dimensional stress. As shown, total radiation efficiency peaks at Mach = 1.0 and decays with further increases in flow speed. It should be noted that the radiation efficiency can decay to a negative value with the radiated power as convection velocity increases. This behavior illustrates the role of coupling on power flow at high convection velocities.
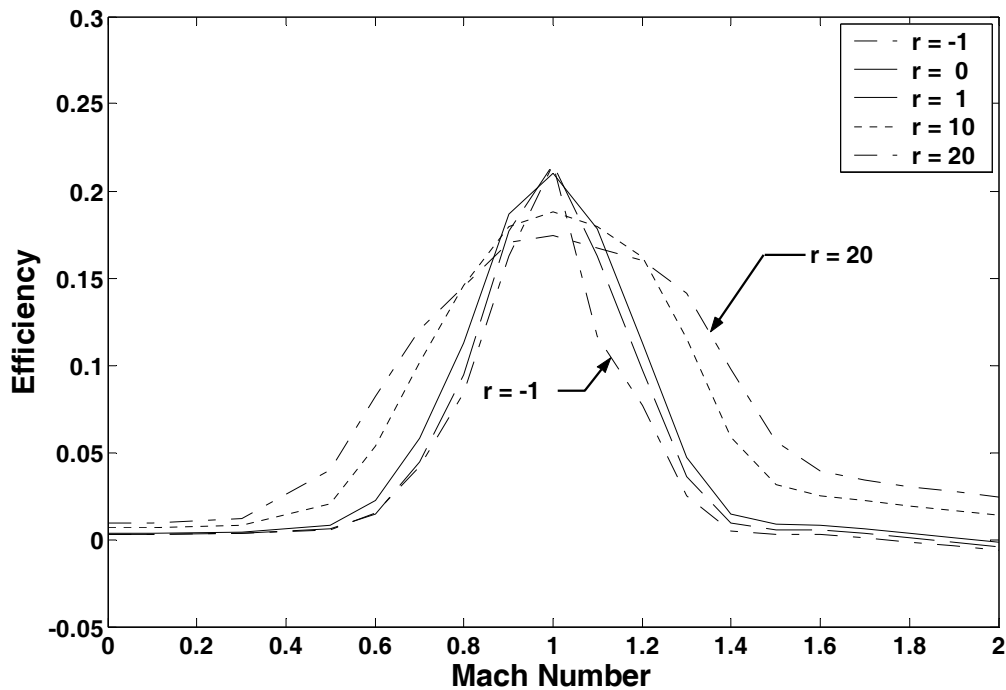
Figure 3-13.   Total radiation efficiency for selected values of non-dimensional stress

The overall behavior of the structure can be summarized by the relationship between radiation efficiency, flow speed and state of stress in the structure. When the

structure is loaded in compression, it exhibits a very narrow range of "efficient" radiation

of energy. Conversely, increasing the value of the in-plane stress has the effect of

widening the range of convection velocities where the structure can be considered an

"efficient" radiator of sound power. Selecting an arbitrary value of 10% as an indication

of efficient radiation, Figure 3-13 shows that there is a minimum range of 10% radiation

efficiency at $r = -1$ (0.8 < Mach Number < 1.2) and a maximum range of 10% efficiency

at $r = 20$ (0.65 < Mach Number < 1.4). It is also interesting that this broadening of the

range of "efficient" radiation is associated with a decrease in peak radiation efficiency.

The efficiency drops from a peak of 21% to a value of 17%. Note that the peak value of

radiation efficiency is associated with a state of compressive stress in the plate and that

this particular plate model had the lowest effective stiffness of any that proved stable

throughout the entire range of convection velocities studied.

Decoupled Subsystems

The Uncoupled Model

Entire texts have been produced dealing with fluid structure interactions[20]. These

works tend to concentrate on problems where analytical solutions are possible. One

commonly used criterion for assuming that analytical techniques are valid is to assume a

low Mach number in the convection velocity. A more definitive criterion is sought for

the method used here. Making this distinction would allow modeling of the system in a

more simplified manner if that approach is desirable.

Figure 2-5 shows the plate and aerodynamic models connected such that the aerodynamic model has a feedback path to the structure. This configuration has been referred to as the *coupled* model. Figure 3-14 shows the alternative connection scheme, where the generalized forces are not feed back into the structural subsystem. This configuration will be referred to as the *uncoupled* model.

When the models are cast in the forms shown in Figures 2-5 and 3-14, the input/output relationships for the system can be easily manipulated and transfer functions between inputs and system variables can be obtained.

In order to make a decision about when the effects of coupling were important to structural response, a criterion had to be selected that provided a decision point. A shift of 5% between the fundamental modal response of the uncoupled model and the coupled model was selected as this criterion. For low values of mass ratio, this coupling boundary is a complex curve, similar to the stability boundary. As the mass ratio increases, the coupling boundary becomes a simple logarithmic relationship.
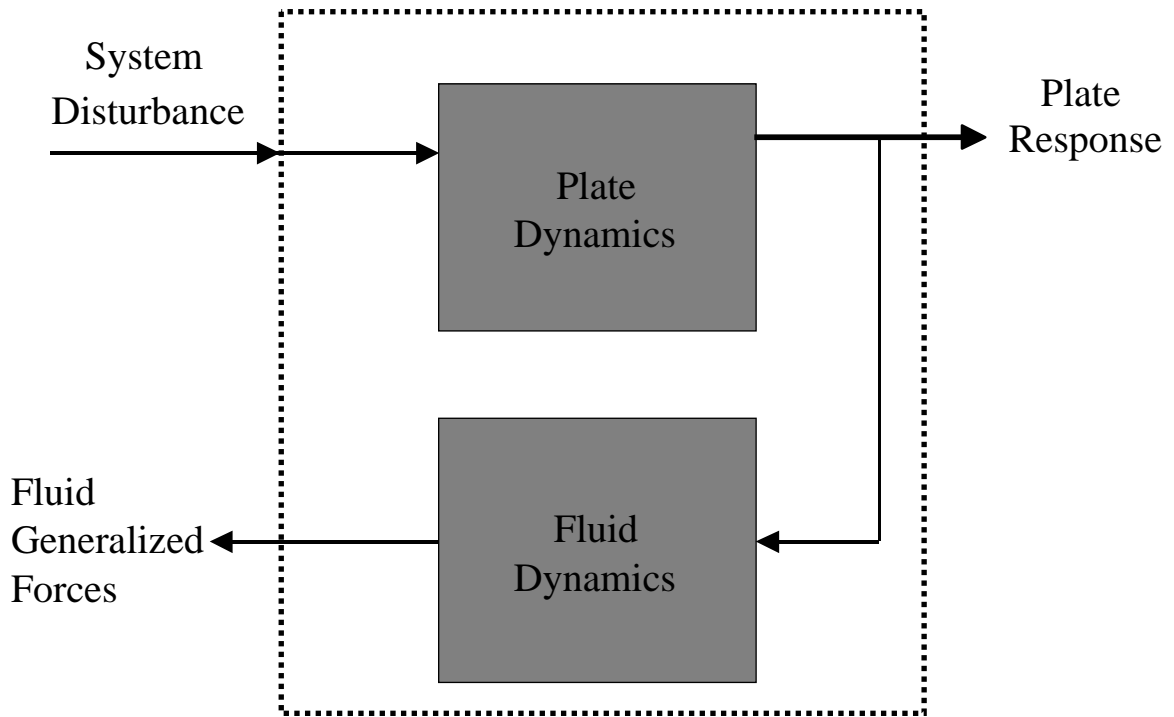
Figure 3-14.   Schematic of the uncoupled fluid / structure system

Specific regions of the parameter space are defined wherein fluid coupling and convection effects must be included for accurate predictions of radiated power. As was done with the structural response, a criterion to determine when coupling was important to calculation of radiated power had to be determined. The threshold of a 15% difference between the total radiation resistance produced by an uncoupled and a coupled model was selected as this criterion. The important result that there is a characteristic flow velocity where coupling the acoustic subsystem to the structural subsystem has a significant effect on radiated power. This flow velocity depends only on the value of the

non-dimensional dynamic pressure with respect to the coupling and stability boundaries and is independent of the value of the mass ratio for many engineering applications.

Non-dimensional Analysis

Structural Response for the Non-dimensional Case

Fluid / structure coupling has been shown to be important in determining both structural response and energy transfer to a convected medium. The studies of fluid structure interactions herein have been confined to specific geometries and fluid parameter sets that characterize a problem of interest. Results from studies of this nature may be narrowly applicable to other problems, but seldom apply directly. The method is now expanded to quantify when the effects of structural / aerodynamic coupling should be considered as a function of non-dimensional parameters. The difference between the coupled and the uncoupled models is the based on the ability of the aerodynamic subsystem to have a feedback path to the structure. This difference is shown schematically in Figures 2-5 and 3-14. The parameters considered in this effort will be non-dimensional dynamic pressure, mass ratio and Mach number. These guidelines can be used in determining the dynamic response and acoustic power radiation associated with a wide range of structures exposed to a wide range of fluids. This is accomplished using dimensionless analysis of both geometric and aerodynamic aspects of the problem. Theoretical development of the equations governing the vibration of a simply supported plate in an infinite baffle and a semi-infinite flowing medium along with the method for coupling these systems is included. Relationships used to render these models non-

dimensional are described in Equations (2-18) – (2-22), and implemented in Equation (2-23).

One effect of employing the coupled model has been shown to be a shift in the frequency of response of the structure. As velocity increases in subsonic flow, it has been shown that the modal response frequencies shift to lower values[13]. Similarly it has also been shown here that in supersonic flow, this trend is reversed, i.e., the modal response frequencies increase as flow velocity increases in magnitude. This behavior has been chosen as the criterion for when the selection of the type of modeling configuration becomes important to structural response. A shift of 5% in fundamental mode frequency when compared to the case of no convection has been chosen as the criterion for determining when coupling significantly effects system behavior. This will be referred to as the *coupling boundary*, denoted as λ_c.

Figure 3-15 shows plots of the stability boundary, λ_S, along with the coupling boundary for selected values of mass ratio. The stability boundary is defined at the limiting value of non-dimensional dynamic pressure, λ, for a given mass ratio, μ, which results in the first occurrence of an unstable pole (first instance of a negative real component of an eigenvalue) for the coupled system at a given Mach number.

For the lower values of mass ratio typical of structures in air, the coupling boundary is a complex curve, similar to the stability boundary for convection velocities of Mach 1.5 and below. A significant jump in the coupling boundary occurs at or around Mach 1.6, indicating some potentially interesting structural aerodynamic interaction in that narrow region of convection velocities associated with a structure of this particular aspect ratio. More detailed study of this portion of the problem is left for a future effort.
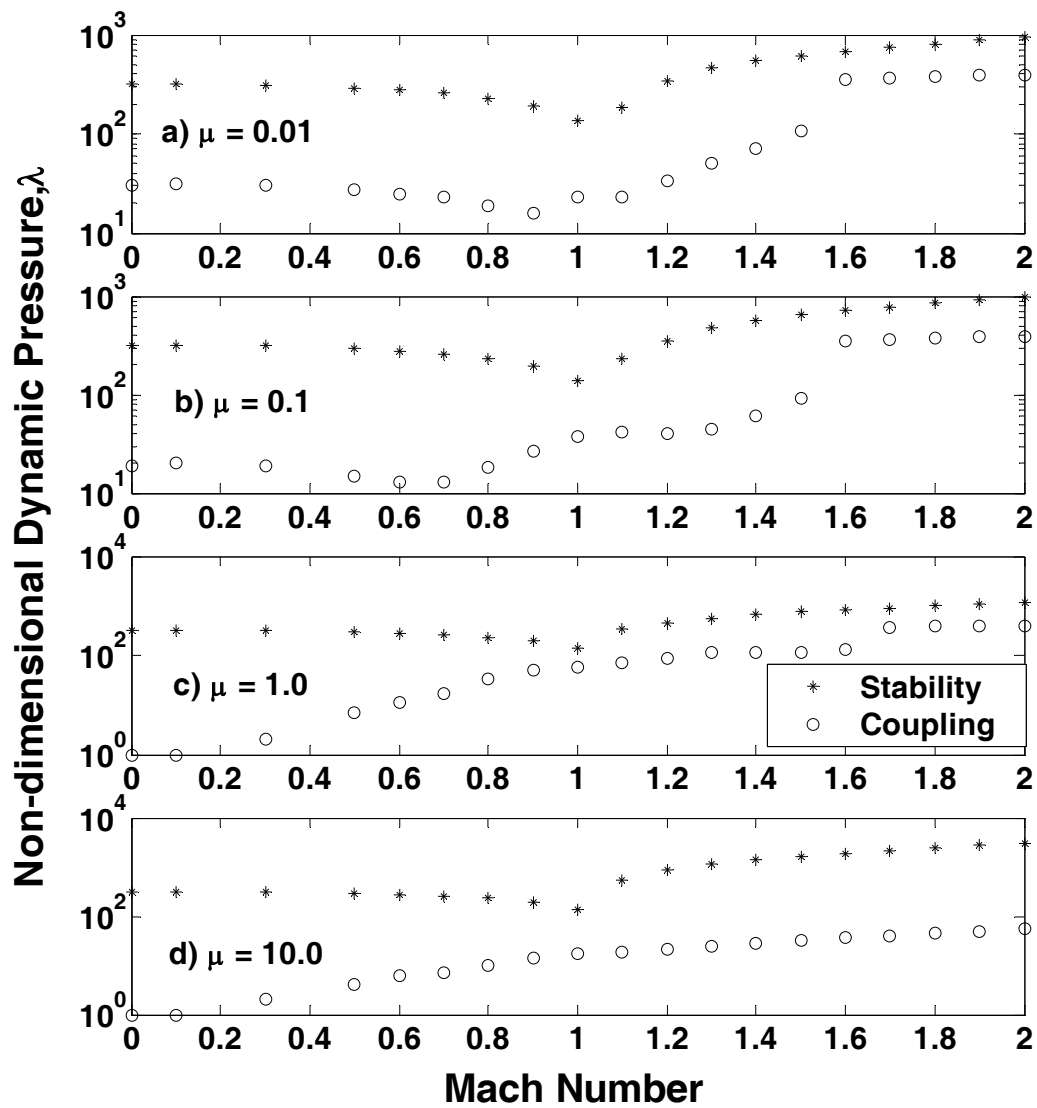
Figure 3-15.   Stability and coupling boundaries for selected values of mass ratio

As mass ratio rises further into areas that would be more typical of heavy structures exposed to water or other dense liquids, the discontinuity in the coupling boundary diminishes and then disappears. For the larger values of mass ratio, the higher convection velocities are not necessarily representative of realistic flow cases, due to the

high velocities represented and the fact that the use of the potential flow model may not be applicable in these regions.

These data suggest that a rough rule of thumb for determining the necessity of using a coupled model to accurately predict structural response would be when λ is a significant fraction of λ_S in lightweight fluids and for most all values of λ in heavy fluids.

Radiation Resistance for the Non-dimensional Case

The radiation resistance has been chosen as a metric for this study because it lends itself well to the non-dimensional format of the problem. Radiation efficiency has been used for dimensional studies of particular geometric and fluid parameter sets. Radiation efficiency is defined as radiation resistance per unit area, and since the plate has no dimensions *per se*, the expression for radiation resistance can be considered a non-dimensional efficiency term.

If accurate prediction of energy flow between the convected medium and the structure is of paramount importance, then a different metric for determining when to use the coupled modeling approach is required. Determining when accurate results using the uncoupled model can be obtained by comparing the power flow characteristics of such a model to the equivalent coupled model and noting where these behaviors begin to diverge significantly.

One effect of this effort has been to show that accurate prediction of radiated power must *always* include the fluid dynamic subsystem in the overall system model. That portion of the system produces the generalized forces on the structure, which is integral to the calculation of radiated power, as shown in Equation (2-77).

The effect on the acoustic radiation of a structure exposed to convection can be characterized by the change in radiation resistance. The radiation resistance, defined in Equation (2-82), is significantly affected by the structure of the system model. In general, an uncoupled model will have a higher radiation resistance than a coupled model. By comparing the difference between the radiation resistance in an uncoupled model with a coupled model, a conclusion can be drawn about when the selection of modeling approach becomes important.

To determine this difference, representative values of λ (non-dimensional dynamic pressure, Equation (2-19)) had to be selected. A total of three values of λ were used to study the behavior of the radiation resistance. λ_c, which was determined in the previous sub-section, was selected to study the effect of frequency shift in the structural response. Two additional values,

$$\lambda_L = \frac{\lambda_c}{2} \tag{3-3}$$

and

$$\lambda_H = \frac{\lambda_S - \lambda_c}{2} \tag{3-4}$$

were evaluated to represent flow regimes well above and well below the selected structural behavior criterion. It is important to recall that these values of non-dimensional pressure are not constant (See Figure 3-15), but change significantly with changes in convection velocity and mass ratio. A value of a 15% difference in radiation resistance between the uncoupled and coupled models was chosen to establish when the difference in energy flow was sufficient to justify using a coupled model.
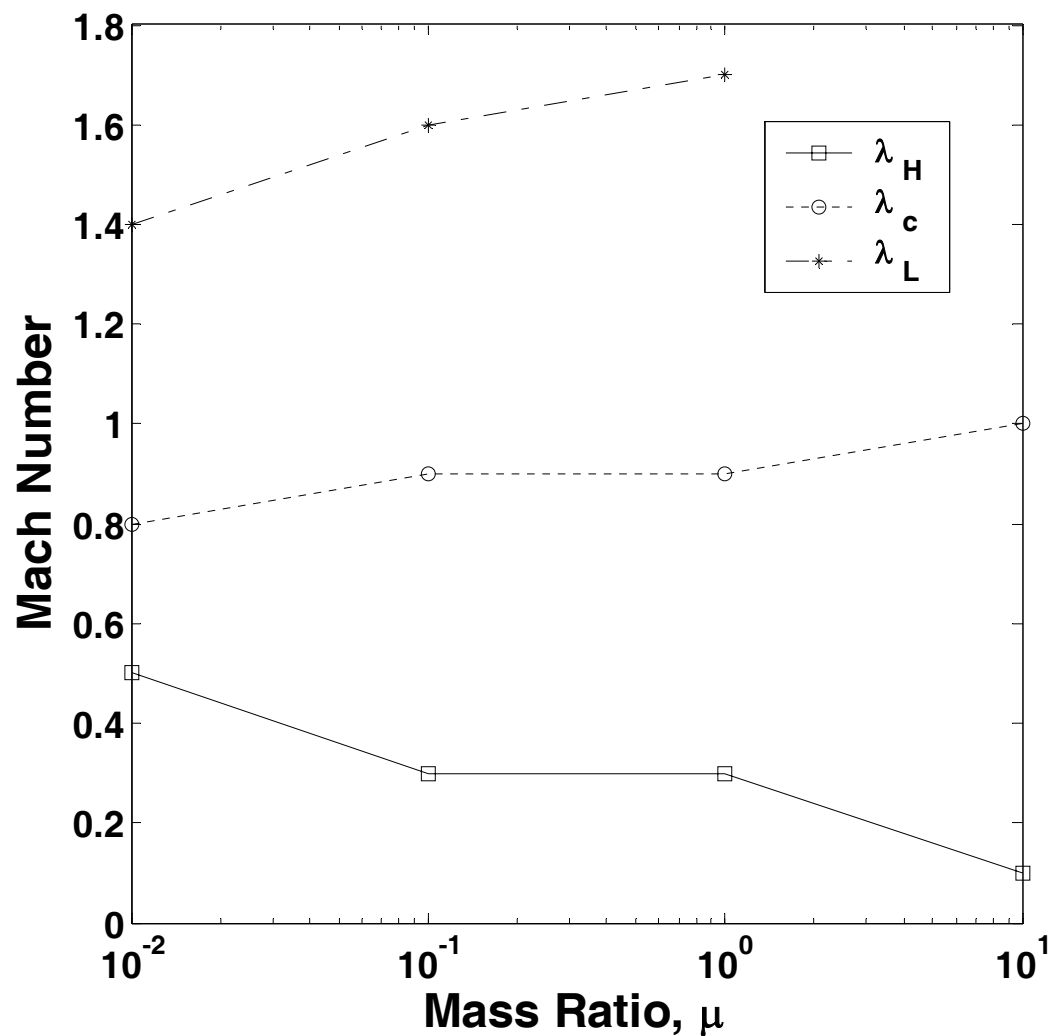
Figure 3-16.   15% Radiation resistance threshold

Figure 3-16 shows a plot of this radiation resistance threshold for the selected

values of non-dimensional dynamic pressure. Note that the mass ratio is the independent

variable in this data, and that the critical values of convection velocity are nearly constant

across the range of mass ratio magnitudes considered here. These results imply that there

is a specific Mach number that determines when coupling is important to determination

of radiated power, based on the system model proximity to the coupling or stability boundary. While a weak dependence on mass ratio is apparent at extremely high and low values of mass ratio, the convection velocity of interest can be assumed to be constant for values of mass ratio commonly encountered in fluid structure interaction scenarios.

Figure 3-16 illustrates a rule of thumb that coupled models should be used when Mach number exceeds 0.3 when the system model is near the stability boundary, when it exceeds 0.8 when the system is in the neighborhood of the coupling boundary. The data also imply that coupling is not important for low values of λ unless the Mach number exceeds 1.5. It should also be noted that for low values of λ and a mass ratio of 10.0, coupling effects were not significant in the range of convection velocities studied.

Based on these findings, the following engineering rules of thumb are proposed:

1. Coupling should be considered for accurate prediction of structural response when $\lambda \cong 10\%$ of λ_S in lightweight fluids and when $\lambda \cong 1\%$ of λ_S in heavy fluids.

2. Coupling should be considered for accurate predictions of radiated power when coupled model eigenvalues are near the stability boundary and flow velocity exceeds Mach = 0.3, when the system eigenvalues are near the coupling boundary and the flow velocity exceeds Mach = 0.8 and for low values of λ and flow velocities exceed Mach = 1.5.

CHAPTER IV

CONCLUSIONS

The effect of flow-induced coupling on the radiated sound power from plates has been presented. The modeling of the plate and fluid has been summarized and the effects of flow-induced coupling on the plate response have been described. The effect of in-plane stress on the radiated sound power from plates has also been discussed. Additionally, a parametric study of non-dimensional structure / convection interaction has been shown. The non-dimensional parameters chosen encompass a wide range of flow regimes and structural configurations.

The first notable effect observed is that the radiated sound power decreases as flow velocities increase from the transonic region. However, the kinetic energy in the plate increases only slightly with flow speed. This behavior is attributable to the flow induced coupling driving some modes out of phase with the aerodynamic model, resulting in decreased radiation. The unstressed structure was also shown to be a net absorber of power when exposed to high convection velocities.

The most interesting effect observed for the stressed structure studied is that total radiation efficiency of the plate is significantly affected by the state of stress in the plate. This effect is manifested as a broadening of the range of convection velocities where the plate is an "efficient" radiator of sound power, and an associated reduction of the peak radiation efficiency. It was also observed that increasing the magnitude of tensile stress

in the plate eliminated the frequency shift in radiated power both in subsonic and supersonic flow

In studying a non-dimensional aerodynamic / structural system model, specific regions of the non-dimensional parameter space have been defined wherein fluid coupling and convection effects must be included for accurate predictions of structural response and radiated power. Utilization of a coupled model is advisable when certain values of non-dimensional pressure are exceeded for a given mass ratio and convection velocity if accuracy of the structural response is of paramount importance. This applies when $\lambda \cong 10\%$ of λ_S in lightweight fluids and when $\lambda \cong 1\%$ of λ_S in heavy fluids. If radiated sound power is the main concern, it was shown that specific convection velocities can be used as a criterion for when a coupled model is desirable for analysis. Specifically, when Mach number exceeds 0.3 and the system model eigenvalues are near the stability boundary, when Mach number exceeds 0.8 when the system is in the neighborhood of the coupling boundary and for low values of λ when the Mach number exceeds 1.5.

REFERENCES

[1] M.C. Junger and D. Feit, *Sound Structures and Their Interaction*, Acoustical Society of America / American Institute of Physics, New York, 1993.

[2] I. D. Abrahams, "Scattering of Sound by an Elastic Plate with Flow," *Journal of Sound and Vibration*, Vol. 89, No. 2, pp. 213-231, 1983.

[3] N. Atalla and J. Nicolas, "A Formulation for Mean Flow Effects on Sound Radiation from Rectangular Baffled Plates with Arbitrary Boundary Conditions," *Journal of Vibration and Acoustics*, Vol. 117, pp. 22-29, 1995.

[4] W. R. Graham, "The effect of mean flow on the radiation efficiency of rectangular plates," *Proceedings of the Royal Society of London*, Vol. 454, pp. 111-137, 1998.

[5] K.D. Frampton, "Radiation efficiency of convected fluid loaded plates," *Journal of the Acoustical Society of America*, Vol. 113, No. 5, pp. 2663-2673, 2003.

[6] L. Meirovitch, *Analytical Methods in Vibrations*, Macmillan Publishing Co., New York, 1967.

[7] A. Berry, "A new formulation for the vibrations and sound radiation of fluid loaded plates with elastic boundary conditions", *Journal of the Acoustical Society of America*, Vol 96, No. 2, Pt. 1, pp. 889-901, 1994.

[8] M.N. Currey and K.A. Cunefare, "The radiation modes of baffled finite plates", *Journal of the Acoustical Society of America*", Vol. 98, No. 3, pp 1570-1580, 1995.

[9] C.E. Wallace, "Radiation resistance of a rectangular panel," *Journal of the Acoustical Society of America*, Vol. 51, No. 3, Part 2, pp. 946-952, 1972.

[10] Earl H. Dowell, *Aeroelasticity of Plates and Shells*, Noordhoff International Publishing, The Netherlands, 1975.

[11] Franck Sgard, Noureddine Atalla and Jean Nicolas, "Coupled FEM-BEM Approach for Mean Flow Effects on Vibro-Acoustic Behavior of Planar Structures," *AIAA Journal*, Vol. 32, No. 12, pp. 2351-2358, 1994.

[12] Sean F. Wu and Lucio Maestrello, "Responses of Finite Baffled Plate to Turbulent Flow Excitations," *AIAA Journal*, Vol. 33, No. 1, pp. 13-19, 1995.

[13] K.D. Frampton, "The effect of flow induced coupling on sound radiation from convected fluid loaded plates", *Journal of the Acoustical Society of America*, Vol. 117, No. 3, pp 1129-1137, 2005.

[14] Frank Fahy, *Sound and Structural Vibration*, Academic Press, New York, 1985.

[15] A. Leissa, *Vibration of Plates*, Acoustical Society of America / American Institute of Physics, New York, 1993.

[16] R.W. Clark, Saunders and G. Gibbs, *Adaptive Structures: Dynamics and Controls*, John Wiley & Sons, New York, New York, 1998.

[17] S. Kung, "A New Identification and Model Reduction Algorithm via Singular Value Decomposition", IEEE 12th Asilomar Conference on Circuits, System and Computers, 1978, pp 705 – 714.

[18] A. Pierce, Acoustics, *An Introduction to It's Physical Principles and Applications*, Acoustical Society of America / American Institute of Physics, New York, 1991

[19] D.J. Johns, *A Manual on Aeroelasticity, Part III, A Panel Flutter Review*, Advisory Group for Aerospace Research and Development (AGARD), Chapter 7, 1969.

[20] M.S. Howe, *Acoustics of Fluid-Structure Interactions*, Cambridge University Press, Cambridge U.K., 1998